J Physiol 587.13 (2009) pp 3251–3269

The Journal of Physiology

Gating, permselectivity and pH-dependent modulation of channels formed by connexin57, a major connexin of horizontal cells in the mouse retina

Nicolas Palacios-Prado[1], Stephan Sonntag[2], Vytenis A. Skeberdis[1], Klaus Willecke[2] and Feliksas F. Bukauskas[1]

[1] *Dominick P. Purpura Department of Neuroscience, Albert Einstein College of Medicine, Bronx, NY 10461, USA*
[2] *Institute of Genetics, Division of Molecular Genetics, University of Bonn, 53117 Bonn, Germany*

Mouse connexin57 (Cx57) is expressed most abundantly in horizontal cells of the retina, and forms gap junction (GJ) channels, which constitute a structural basis for electrical and metabolic intercellular communication, and unapposed hemichannels (UHCs) that are involved in an exchange of ions and metabolites between the cytoplasm and extracellular milieu. By combining fluorescence imaging and dual whole-cell voltage clamp methods, we showed that HeLa cells expressing Cx57 and C-terminally fused with enhanced green fluorescent protein (Cx57-EGFP) form junctional plaques (JPs) and that only cell pairs exhibiting at least one JP demonstrate cell-to-cell electrical coupling and transfer of negatively and positively charged dyes with molecular mass up to ∼400 Da. The permeability of the single Cx57 GJ channel to Alexa fluor-350 is ∼90-fold smaller than the permeability of Cx43, while its single channel conductance (57 pS) is only 2-fold smaller than Cx43 (110 pS). Gating of Cx57-EGFP/Cx45 heterotypic GJ channels reveal that Cx57 exhibit a negative gating polarity, i.e. channels tend to close at negativity on the cytoplasmic side of Cx57. Alkalization of pH_i from 7.2 to 7.8 increased gap junctional conductance (g_j) of ∼100-fold with $pK_a = 7.41$. We show that this g_j increase was caused by an increase of both the open channel probability and the number of functional channels. Function of Cx57 UHCs was evaluated based on the uptake of fluorescent dyes. We found that under control conditions, Cx57 UHCs are closed and open at $[Ca^{2+}]_o = \sim 0.3$ mM or below, demonstrating that a moderate reduction of $[Ca^{2+}]_o$ can facilitate the opening of Cx57 UHCs. This was potentiated with intracellular alkalization. In summary, our data show that the open channel probability of Cx57 GJs can be modulated by pH_i with very high efficiency in the physiologically relevant range and may explain pH-dependent regulation of cell–cell coupling in horizontal cell in the retina.

(Received 26 February 2009; accepted after revision 7 May 2009; first published online 11 May 2009)
Corresponding author F. F. Bukauskas: Dominick P. Purpura Department of Neuroscience, Albert Einstein College of Medicine, Bronx, NY 10461, USA. Email: fbukausk@aecom.yu.edu

Abbreviations A_h, coefficient characterizing the steepness of g_j decay of AHC over V_j; AHC, apposed hemichannel; AF^{350}, Alexa Fluor-350; F_{JP}, fluorescence per unit area in *en face* JPs; F_γ, fluorescence produced by a single GJ channel; F_T, total fluorescence of JP; $\gamma_{h,o}$, unitary conductance of AHC at the fully open state; $\gamma_{h,res}$, unitary conductance of AHC at the residual state; γ_o, unitary conductance of GJ channel at the fully open state; γ_{res}, single channel conductance at the residual state; JP, junctional plaque; g_j, transjunctional conductance; GJ, gap junction; AHC_R and AHC_L, right- and left-side AHCs; K, fraction of operating channels at any given time; MKR, modified Krebs–Ringer solution; N_T, total number of physical channels in a JP; N_f, number of functional channels; O–O, both AHCs are in the open state; C–C, both AHCs are in the closed state; O–C and C–O, one AHC is in the open state, while the other AHC is in the closed state; P_j, junctional permeability; P_γ, single channel permeability; ROI, region of interest; $P_{o\text{-}o}$, $P_{o\text{-}c}$, $P_{c\text{-}o}$ and $P_{c\text{-}c}$, probabilities of channels to dwell in O–O, O–C, C–O and C–C states, respectively; UHC, unapposed hemichannel; $V_{h,o}$, V_j at which equilibrium constant between states of AHCs are equal to 1; V_h, voltage across AHC; V_j, transjunctional voltage.

DOI: 10.1113/jphysiol.2009.171496

Connexins (Cxs), a large family of membrane proteins, form gap junction (GJ) channels that provide a direct pathway for electrical and metabolic signalling between cells (Harris, 2001; Sohl *et al.* 2005). The docking of two apposed hemichannels (AHCs) at the cell–cell contact forms a GJ channel. Connexin-based hemichannels found at the non-junctional plasma membrane, called unapposed hemichannels (UHCs), connect the cell interior with the extracellular milieu. They have been implicated in physiological functions including paracrine intercellular signalling and induction of cell death under pathological conditions (Saez *et al.* 2003). Functional properties of Cx-based channels vary notably depending on the Cx isoform and can be modulated by voltage, phosphorylation, $[Ca^{2+}]_i$, pH, arachidonic acid and many other lipophilic uncouplers (Baldridge *et al.* 1987; Bennett *et al.* 1991; Bukauskas & Verselis, 2004; Jouhou *et al.* 2007*b*).

The retina is a highly organized laminar structure with three nuclear layers where cell bodies are located and two plexiform layers where the dendritic interactions take place. Seven major cell types compose the retinal layers and most of them exhibit gap junctional communication (Vaney & Weiler, 2000). Neurobiotin cell–cell transfer studies have revealed extensive coupling between horizontal, bipolar, amacrine or photoreceptor cells (McMahon *et al.* 1989; Becker *et al.* 1998; Hombach *et al.* 2004). Several Cx isoforms, such as Cx30.2, Cx36, Cx37, Cx43, Cx45 and Cx57, have been reported to be expressed in the mouse retina with a cell type-dependent expression pattern (Sohl *et al.* 2005; Kreuzberg *et al.* 2008). In addition, it was concluded that Cx26 is expressed in the horizontal cells of carp (Janssen-Bienhold *et al.* 2001) but not mice (Deans & Paul, 2001).

The first excitatory synaptic relay within the retinal circuit is located in the outer plexiform layer where photoreceptors project to horizontal and bipolar cells. The lateral contacts between photoreceptors and horizontal cells are thought to be the origin of a feedback pathway that modulates light adaptation and luminance contrast, and forms the basis of the centre–surround antagonism of bipolar and ganglion cells (Kuffler, 1953); for review see (Kamermans & Spekreijse, 1999). Several hypotheses for this feedback have been proposed including a GABA-dependent pathway (Kaneko & Tachibana, 1986), changes in the concentration of hydrogen ions in the synaptic cleft of the photoreceptor terminal (Hirasawa & Kaneko, 2003; Davenport *et al.* 2008; Vessey *et al.* 2005; Cadetti & Thoreson, 2006; Jouhou *et al.* 2007*a*) and hemichannel-mediated ephaptic inhibition of photoreceptors (Kamermans *et al.* 2001; Kamermans & Fahrenfort, 2004). It was reported that horizontal cells form a large syncytial network in the mouse retina via GJs formed for the most part of Cx57 (Hombach *et al.* 2004; Ciolofan *et al.* 2007; Janssen-Bienhold *et al.* 2009). This gap junctional communication between horizontal cells has been considered a structural substrate for a large receptive field (Hampson *et al.* 1992). Gap junctional communication between horizontal cells can be modulated by multiple neuromodulators (McMahon, 1994; Mills & Massey, 1995; Weiler *et al.* 2000), arachidonic acid (McMahon, 1994), $[Ca^{2+}]_o$ (Teranishi *et al.* 1983; 1984; Gallemore *et al.* 1994; Rabl & Thoreson, 2002) and pH (DeVries & Schwartz, 1989; Hampson *et al.* 1992; Jouhou *et al.* 2007*b*). However, studies with Cx57 knockout mice have suggested that Cx57 expression may not be critical for spatial tuning and light adaptation of ganglion cells (Dedek *et al.* 2008) although receptive field size and resting potential of horizontal cells are affected (Shelley *et al.* 2006). Despite extensive studies performed on this matter, the nature of the feedback and role of Cx57 in the mouse retina remains a subject of discussion.

We analysed HeLa transfectants expressing wild-type Cx57 or Cx57 fused to its C-terminus with an enhanced green fluorescent protein (Cx57-EGFP). Originally, it was reported that Cx57 is coded by a single exon and HeLa cells expressing Cx57 were generated based on the predicted sequence. Their electrical and permselectivity properties were addressed in Manthey *et al.* (1999). Later, DNA studies in mouse horizontal cells revealed that Cx57 is coded by a second exon spliced to the coding region of the first exon causing a shorter carboxy-terminal region (Hombach *et al.* 2004). Using combined fluorescence imaging and dual whole-cell patch clamp methods, we examined the voltage gating, permselectivity and pH-dependent modulation of GJ channels in HeLa cells expressing the corrected sequence of Cx57. Functional properties of Cx57 UHCs were evaluated based on dye uptake during time-lapse imaging over ∼5 h. We found similar voltage gating properties as previously reported (Manthey *et al.* 1999) but with higher single channel conductance. Under control conditions at pH_i 7.2, junctional conductance (g_j) was very low, and g_j increased ∼100-fold during relatively weak intracellular alkalization. We found that this g_j increase was caused by a reduction of V_j-gating sensitivity of AHC and an increase in the number of functional GJ channels. In addition, dye uptake through Cx57 UHCs increased at moderately low levels of $[Ca^{2+}]_o$ (∼0.3 mM or below) and is potentiated by intracellular alkalization.

Methods

Cloning of retinal Cx57

A pMJ-Cx57eGFP vector was generated for transfection of HeLa cells. Briefly, a *Nco*I/*Bam*HI mouse Cx57 PCR fragment (Position 1 to 1476) (Hombach *et al.* 2004) was cloned into the *Nco*I/*Bam*HI sites of pMJGreen (Maxeiner *et al.* 2005), which contained the CMV

promoter, a polyadenylation signal and a gene that conferred resistance to puromycin. To generate the pMJ-Cx57-IRES-eGFP vector, the *Nco*I/*Bam*HI fragment of Cx57 and an *Eco*RI/*Not*I fragment of IRES-eGFP from pIRES-eGFP-zeo+ (Dobrowolski *et al.* 2007) were cloned into the *Nco*I/*Not*I sites of pMJ-Green.

Cells and culture conditions

Experiments were performed using HeLa cells (human cervix carcinoma cells, ATCC CCL2). Cells were grown in Dulbeco's modified Eagle's medium supplemented with 8% fetal calf serum, 100 μg ml^{-1} streptomycin and 100 units ml^{-1} penicillin. Cells were maintained in the CO_2 (5%) incubator at 37°C. For the transfection procedure we used 2 μg of pMJ-Cx57eGFP or pMJ-Cx57-IRES-eGFP DNA and Lipofectamine2000 (Invitrogen, Carlsbad, CA, USA) following the manufacturer's protocol. Clones were selected after cells were grown in the presence of puromycin, 1 μg ml^{-1} (Sigma, Dreisenhofen, Germany).

Electrophysiological recordings and analysis

Experiments were performed in a modified Krebs–Ringer (MKR) solution containing (in mM): NaCl, 140; KCl, 4; $CaCl_2$, 2; $MgCl_2$, 1; glucose, 5; pyruvate, 2; Hepes, 5 (pH 7.4). Electrodes were filled with a pipette solution containing (in mM): KCl, 140; NaAsp, 10; MgATP, 3; $MgCl_2$, 1; $CaCl_2$, 0.2; EGTA, 2; Hepes, 5 (pH 7.2). For simultaneous electrophysiological and fluorescence recordings, cells were grown onto glass coverslips and transferred to an experimental chamber mounted on the stage of an inverted microscope (Olympus IX70) equipped with a fluorescence imaging system. Cells were perfused with MKR solution at room temperature. Junctional conductance (g_j) was measured in selected cell pairs using the dual whole-cell patch clamp system. Briefly, each cell of a pair was voltage clamped independently with a separate patch clamp amplifier. Transjunctional voltage (V_j) was induced by stepping the voltage in cell-1 (ΔV_1) and keeping the other constant, $V_j = \Delta V_1$. Junctional current (I_j) was measured as the change in current in the unstepped cell-2, $I_j = \Delta I_2$. Thus, g_j was obtained from the ratio $-I_j/V_j$, where the negative sign indicates that the junctional current measured in cell-2 is oppositely oriented to the one measured in cell-1. To avoid effects of series resistance on g_j measurements (Wilders & Jongsma, 1992), we selected cell pairs exhibiting typically small junctional plaques (JP), and maintained the pipette resistances below 5 MΩ. Typically, cell pairs without JPs showed no coupling. Signals were acquired and analysed using custom-made software (Trexler *et al.* 1999) and A/D converter from Axon Instruments.

Fluorescence imaging and dye transfer studies

Fluorescence signals were acquired using an ORCA digital camera (Hamamatsu Corp., Bridgewater, NJ, USA) with UltraVIEW software for image acquisition and analysis (Perkin Elmer Life Sciences, Boston, MA, USA).

For dye transfer studies, a given dye was introduced into cell-1 of a pair through a patch pipette in whole-cell voltage clamp mode. Dyes used include (molecular mass of the fluorescent ion, valence): Lucifer yellow (LY) (443, −2), Alexa Fluor-350 (AF^{350}) (326, −1), ethidium bromide (EtBr) (314, +1), DAPI (279, +2) and propidium iodide (PrI) (415, +2) (Invitrogen, Eugene, OR, USA). Typically, this resulted in a rapid loading of cell-1 followed by dye transfer to the neighbouring cell-2. In our earlier studies of single channel permeability of GJs, a whole cell recording in the dye recipient cell (cell-2) was established ∼6–10 min after opening the patch in cell-2. This allowed us to measure g_j and avoid dye loss due to its diffusion from cell-2 to the patch pipette.

To account for changes of fluorescence intensity in both cells as well as g_j we used the Goldman–Hodgkin–Katz (GHK) equation (Hille, 2001) adapted for junctional permeability (P_j) measurements (Verselis *et al.* 1986). The transjunctional flux (J_j) of dye through gap junction channels is determined by change in dye concentration in cell-2 (ΔC_2) over time interval (Δt) so that:

$$J_j = \mathrm{vol}_2(\Delta C_2/\Delta t) \quad (1)$$

where vol_2 is the volume of cell-2. Then, according to a modified GHK equation (Verselis *et al.* 1986), the total junctional permeability (P_j) can be described as follows:

$$P_j = \frac{J_j[1 - \exp(-zFV_j/RT)]}{(zFV_j/RT)\,[C_1 - C_2\exp(-zFV_j/RT)]} \quad (2)$$

where z is the net charge of dye molecule, F is Faraday's constant, R is the gas constant, T is absolute temperature, and C_1 and C_2 are dye concentrations in cell-1 (dye-donor) and cell-2 (dye-recipient), respectively. In the present study, we examined P_j in the absence of a transjunctional electrical field ($V_j = 0$ mV). Therefore, eqn (2) can be transformed as follows:

$$P_j = \frac{J_j}{C_1 - C_2} = \frac{\mathrm{vol}_2(\Delta C_2/\Delta t)}{C_1 - C_2} \quad (3)$$

As we indicate below, g_j of Cx57-EGFP junctions at control (normal) conditions was relatively low and to improve dye transfer, we used ammonium chloride. Under these conditions we needed to measure g_j continuously. However, when both patch pipettes are in the whole-cell recording mode, a fraction of dye molecules that are transferred to the cell-2 through GJ channels will diffuse to the patch pipette on cell-2. This can be accounted by writing an equation in which a change of the concentration

in the cell-2 (ΔC_2) over time Δt is described as follows:

$$\frac{\Delta C_2}{\Delta t} = \frac{P_j(C_1 - C_2) - (P_p C_2)}{\text{vol}_2} \quad (4)$$

where P_p is the permeability of dye from cell-2 to pipette-2 (see eqn (7)). Then from eqn (4) it follows:

$$P_j = \frac{(\text{vol}_2 \Delta C_2/\Delta t) + P_p C_2}{C_1 - C_2} \quad (5)$$

Cell volume was approximated as a hemisphere. The diameter of a hemisphere was determined by averaging the longest and the shortest diameters of the cell; on average, the volume of examined HeLa cells was $\sim$1800 μm^3. Assuming that dye concentration (C) is directly proportional to fluorescence intensity (FI) ($C = k \times \text{FI}$), which for a number of anionic dyes at concentrations below 1 mM is supported by our studies as well as others (Valiunas *et al.* 2002; Ek-Vitorin & Burt, 2005), then eqn (5) can be modified as follows:

$$P_j = \frac{(\text{vol}_2 \Delta \text{FI}_2/\Delta t) + P_p \text{FI}_2}{\text{FI}_1 - \text{FI}_2} \quad (6)$$

where $\Delta \text{FI}_2 = \text{FI}_{2,n+1} - \text{FI}_{2,n}$ is the change in FI in cell-2 over the time, $\Delta t = (t_{n+1} - t_n)$; n is nth time point in the recording. P_p depends mainly on the size of the tip of the patch pipette. To estimate P_p we blocked gap junctional conductance by heptanol or another gap junction channel blocker and measured the kinetics of FI_2 decay over time. Under blocking conditions, $P_j = 0$ and from eqn (6) it follows that:

$$P_p = \frac{-\text{vol}_2(\Delta \text{FI}_2/\Delta t)}{\text{FI}_2} \quad (7)$$

We used this equation to estimate P_p under blocking conditions of gap junctional communication and our data show that it varies in the range of $\sim$1–3 $\times$ 10^{-11} cm^3 s^{-1}. For more details see the section describing P_j measurements and Fig. 7B. Single channel permeability (P_γ) can be found by dividing P_j by the number of functional channels ($N_f = g_j/\gamma$, where γ is the single channel conductance) at any given time:

$$P_\gamma = \frac{P_j}{g_j/\gamma} = \frac{(\text{vol}_2 \Delta \text{FI}_2/\Delta t) + P_P \text{FI}_2}{(\text{FI}_1 - \text{FI}_2) N_f} \quad (8)$$

To increase dye detection sensitivity, which is particularly important in cases where coupling is weak and/or channel permeability is low, time-lapse imaging was performed as follows: the entire visible field was exposed to excited light followed by focused excitation light directed only at the dye-recipient cell. The latter allowed us to avoid emission light scattering from the dye-donor cell as well as from the dye-filled pipette, which can obscure dye transfer to the recipient cell in cases where permeability is low or can give the appearance of dye transfer when it is, in fact, absent. Our estimates show that when using this approach, the sensitivity of dye transfer measurements increases over 100-fold compared with traditional methods when both cells are exposed to excitation light.

To minimize dye bleaching, we performed time-lapse imaging exposing cells to a low-intensity light for $\sim$0.5 s every 6 s or more. We also used low dye concentrations in a pipette solution, typically 0.1 mM and below, which minimized photo toxicity, but still provided satisfactory fluorescence intensities. We found no difference in fluorescence intensity over time when images were acquired once every 20 s or every 6 s, indicative that dye bleaching was minimal. We have used a similar methodology for evaluation of single channel permeability of connexins 30.2, 40, 43 and 45 (Rackauskas *et al.* 2007).

To study whether Cx57 forms functional UHCs, we examined an uptake of fluorescent dyes using time-lapse imaging over $\sim$5 h. Cells were plated in a 35 mm thin glass-bottomed ($\sim$0.1 mm) Petri dish and placed on the top of $\times$40 or $\times$60 oil objective inside the CO_2 microincubator adapted to fit on the stage of an inverted microscope. Temperature was maintained at 37°C and the microincubator was filled with humidified air when cells were exposed to MKR solution and with air containing 5% CO_2 when cells were exposed to Dulbecco's modified Eagle's medium (DMEM) with 8% fetal bovine serum (FBS). Time-lapse imaging over several days showed that cells grew normally with a proliferation rate similar to that in a standard CO_2 incubator. This set-up has been used previously to examine the function of Cx30.2, Cx31.9, Cx40, Cx45 and Cx43 UHCs (Contreras *et al.* 2003; Bukauskas *et al.* 2006). Repeated series of images were taken with an exposure time of 500 ms by using different excitation and emission filter sets; interlapse interval was $\sim$5–10 min. Selected filters were housed in Sutter filter wheels (LAMBDA 10-2) and their positioning was controlled by the imaging software.

Data analysis and statistics

The analysis was performed using SigmaPlot software and averaged data are reported as the mean ± S.E.M.

Results

Electrical cell–cell coupling and voltage gating

Experiments were performed using spontaneously preformed HeLaCx57-EGFP cell pairs exhibiting one or several small JPs by measuring g_j with a double-voltage clamp method. We found that cell pairs exhibiting JPs were electrically coupled and demonstrated full uncoupling under exposure to heptanol (2 mM), octanol (0.5 mM)

or CO_2. Thus, Cx57-EGFP GJ channels show similar properties to other members of the connexin family.

In examined cell pairs, JPs varied in size from small puncta with a diameter less than 1 μm to very large JPs up to 5 μm or more in length occupying almost the entire region of cell–cell contacts. Figure 1*A* and *B* shows two cells pairs with small (*A*) and large (*B*) JP in the contact region between two cells. At control conditions, g_j varied between ~0.01 and 2 nS with a mean value of $\sim 0.39 \pm 0.18$ nS ($n = 39$). There was no coupling in cell pairs without JPs ($n = 4$; not shown) and, in general, g_j was higher in cell pairs with larger JPs. On average, g_j values in HeLaCx57-EGFP cell pairs were ~500-fold lower than in HeLaCx43-EGFP cell pairs (Bukauskas *et al.* 2000) exhibiting JPs of similar size, which allowed us to assume that only a small fraction of Cx57 GJ channels are functional.

Under control conditions, the averaged g_j was very low and it was difficult to obtain stable recordings over the time needed to study V_j-gating. As we show below, g_j of Cx57-EGFP cell pairs depends on pH_i. To increase quality of the records illustrating V_j-gating, we increased pH of the pipette solution from 7.2 to 7.3. This increased g_j up to several nanosiemens allowing us to study V_j-gating relatively stably. Figure 2*B* shows an average g_j–V_j plot from four consecutive measurements in one Cx57-EGFP cell pair by applying V_j ramps that change from 0 to −110 mV and from 0 to +110 mV (Fig. 2*A*). It shows a symmetric bell shaped dependence. Similar g_j–V_j plots were obtained in seven other cell pairs. To determine gating parameters, we fitted the g_j–V_j dependence with a stochastic four state model of contingent gating (Paulauskas *et al.* 2009); below it is called as *the model of contingent gating*. In the model, each AHC contributes one fast voltage-sensitive gate. Transitions between open and closed states of AHC (gates) are described by the equilibrium constant (K_i), which depend on A_h, the coefficient characterizing sensitivity to voltage across AHC (V_h), and $V_{h,o}$, which is the value of V_h at which $K_i = 1$. When both AHCs are open (O–O), each with conductance $\gamma_{h,o}$, then the GJ channel is in the fully open state with conductance γ_o determined by two $\gamma_{h,o}$ values in series. When both AHCs are closed (C–C), each with conductances $\gamma_{h,res}$, then the GJ channel is in the residual state with conductance γ_{res} determined by two $\gamma_{h,res}$ values in series. Intermediate states (C–O and O–C) contributed conductances determined by $\gamma_{h,o}$ and $\gamma_{h,res}$ in series. Therefore, two voltage gates in series control the gating of GJ channels in a contingent manner, when gating of one AHC depends on the state of the other AHC. We assumed that for Cx57 hemichannels $\gamma_{h,o} = 114$ pS (twice higher than conductance of GJ channel, $\gamma_o = 57$ pS; see below). Conductance of the residual state, $\gamma_{h,res}$, we left variable and evaluated from the fitting process. This was done due to the fact that the model accounts for only the fast gating mechanism while GJ channels also contain the slow gating mechanism, which closes channels fully (Bukauskas & Verselis, 2004). The ratio between activation of the fast and the slow gating mechanisms is unknown, and the fitting process should return some averaged value between $\gamma_{h,res}$ and zero conductance. The grey line in Fig. 2*B* shows the fitting curve of the g_j–V_j plot using the following set of parameters of the model: $A_R = 0.054$ mV^{-1}; $A_L = 0.057$ mV^{-1}; $V_{oR} = -9$ mV; $V_{oL} = -10$ mV; $N_f = 270$, where the R and L subscripts describe the gating parameter for the right- and left-side AHC, respectively, and N_f is the number of functional GJ channels. Least-squares criteria were used to optimize the fitting. Figure 2*C* and *D* shows dependencies of different parameters on V_j: (1) $g_{h,R}$–V_j and $g_{h,L}$–V_j dependencies of left- and right-side AHCs, where $g_{h,R}$ and $g_{h,L}$ integrate conductances of both open and closed AHCs (grey and black lines, respectively; in Fig. 2*C*); (2) the probability of GJ channels to dwell in the O–O state ($P_{o\text{-}o}$, black line; in Fig. 2*D*); (3) the probability of GJ channels to dwell in the C–O, O–C or C–C state ($P_{o\text{-}c}$, $P_{c\text{-}o}$ and $P_{c\text{-}c}$, grey lines; in Fig. 2*D*). If all 270 GJ channels are fully open ($P_{o\text{-}o} = 1$), then g_j should be equal 15.4 nS. However, due to low $P_{o\text{-}o}$ (~0.14), measured g_j was much lower (~2.1 nS). The C–O, O–C and C–C states also contribute to the measured g_j but to a much lower extent due to their lower unitary conductances.

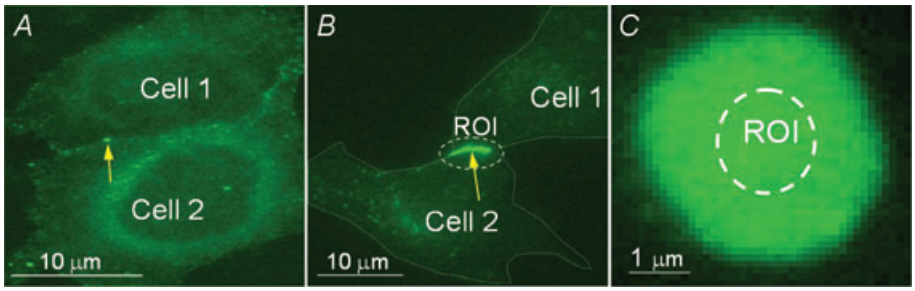

Figure 1. Representative images showing junctional plaques in cell pairs expressing Cx57-EGFP
A–B, fluorescence images of cell pairs with small (*A*) and large (*B*) JPs (see arrows). *C*, fluorescence image of the region where cells overlap and form large JP oriented parallel to the focal plane. Areas encircled with dashed lines are regions of interest (ROI) where fluorescence intensity was measured.

Figure 2*E* shows an example of I_j recorded in response to repeated V_j ramps (±15 mV) and step (+75 mV) in a Cx57-EGFP cell pair (pH_i 7.3). In response to a V_j step, g_j declined from ∼8.4 to 2 nS over ∼2–3 s (bottom trace). Repeated V_j ramps allow the tracking of g_j recovery after each V_j step. The enlarged g_j trace in the inset distinguishes the fast and slow phases in the g_j recovery with a time constant of ∼0.3 s and 2.6 s, respectively. In concert with our earlier reports (Bukauskas & Verselis, 2004), these data allow us to assume that the fast phase reflects the fraction of GJ channels closed by the fast gate and the slow phase reflects channels closed by the slow gate. Therefore, those data support the view that both fast and slow gating mechanisms are involved in the voltage gating of Cx57-EGFP GJs.

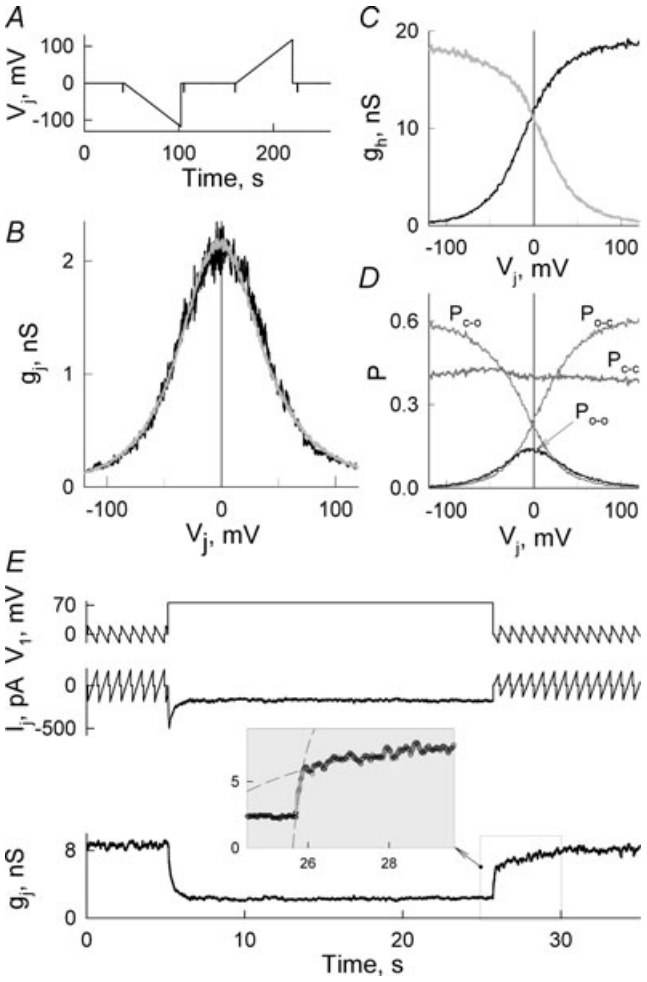

Figure 2. Voltage gating of Cx57-EGFP gap junction channels
A–B, g_j–V_j dependence (*B*) measured in Cx57-EGFP cell pair by applying 60 s long V_j ramps (*A*). The fitting curve shown in grey (*B*) was obtained by using the model of contingent gating. *C*, g_h–V_j dependencies of left- and right-side AHCs (grey and black lines, respectively) integrating conductances of open and gated AHCs. *D*, probability of channels to dwell in different states (O–O, C–O, O–C and C–C) depending on V_j. Black line shows $P_{o\text{-}o}$, while grey lines show $P_{c\text{-}o}$, $P_{o\text{-}c}$, and $P_{c\text{-}c}$. *E*, an example of V_j-gating of Cx57-EGFP cell pair. The bottom trace shows dynamics of g_j calculated from V_j and I_j traces. g_j decayed in response to V_j step of +75 mV. Measurements of g_j during repeated V_j ramps (±15 mV) show that g_j recovery after V_j step has two distinct phases: fast and slow. Dashed lines in the inset show the fitting curves to a single exponential function of the data in periods corresponding to the fast and slow phases of g_j recovery. Time constants of the fast and the slow phases were ∼0.3 and 2.6 s, respectively.

Single gap junction channel

In a cell pair exhibiting low coupling at pH_i 7.2, I_j recordings frequently revealed unitary gating events ($n = 5$). Figure 3*A* demonstrates I_j transitions between the open state with conductance (γ_o) and the substate, also called residual state, with conductance (γ_{res}) during a V_j step of −95 mV. The inset in Fig. 3*A* shows the calculated g_j for the time window between 64 and 78 s, where several unitary gating events took place. The frequency histogram (top-right) revealed two major peaks of 11.0 ± 0.9 and 57.0 ± 1.4 pS, which presumably correspond to γ_{res} and γ_o, respectively. In Fig. 3*A* can be seen simultaneous opening of two GJ channels (see arrow). Theoretically, the open channel probability (P_o) of Cx57 can be calculated dividing the nominal open probability (NP_o) by the number of functional GJ channels (N_f) estimated from simultaneous opening events from the I_j record. Following this concept, we found that at V_j values in between of 80 and 100 mV $P_o = 0.06 \pm 0.02$ ($n = 4$). However, P_o depends on applied V_js and cannot be measured at $V_j = 0$ mV. To overcome these problems at least in part, we used the model of contingent gating (Paulauskas *et al.* 2009). We simulated unitary gating events similar to those shown in Fig. 3*A*. Figure 3*B* shows the simulated I_j record using parameters close to those obtained during fitting of the g_j–V_j plot shown in Fig. 2*B*, which were obtained at a similar pH_i (7.2 *vs.* 7.3). We found that unitary events shown in *B* can be observed by measuring I_j in a cell pair containing 200 functional GJ channels exhibiting $V_{h,o} = -20$ mV and $A_h = 0.085$ mV^{-1}. Figure 3*C* shows the dependencies of probabilities of channels to dwell in different states on V_j. Therefore, even though $N_f = 200$, only two simultaneous opening events were detected (see arrows) during a 100 s period of simulation because $P_{o\text{-}o}$ at $V_j = 95$ mV was very low (∼0.002).

The I_j record from another cell pair exhibiting single channel events in response to three consecutive V_j ramps of ±80 mV is shown in Fig. 3*D*. The continuous lines are drawn over the I_j values corresponding to the open states of one and two channels. The linear character of the I_j over V_j indicates that the open state shows no rectification (Fig. 3*E*). In this cell pair, we observed gating transitions of ∼43–49 pS to the residual state (see dashed line), as well as transitions of ∼57 pS to the close state (see arrow). We assume that the transitions of 43–49 pS in amplitude

were operated by the fast gating mechanism and the transitions of ∼57 pS in amplitude were operated by the slow or the 'loop' gating mechanism (Bukauskas & Verselis, 2004). Therefore, gating to γ_{res} at the single channel level, as well as data shown in Fig. 2*B* allow us to conclude that tagged EGFP does not suppress function of the fast gating mechanism of Cx57, as it was reported for Cx43 (Bukauskas *et al.* 2001).

In summary, we found that an estimation of unitary conductances was much more challenging for Cx57 compared to many other Cx isoforms that have been studied (Bukauskas & Verselis, 2004). We assume that due to a very low $P_{o\text{-}o}$ under control conditions, a substantial number of GJ channels should be functional to observe unitary gating events.

pH_i-dependent modulation of the cell–cell coupling and voltage gating

Figure 4*A* shows the dynamics of I_j and g_j at $V_j = 0$ mV measured by applying repeated V_j ramps of ±20 mV

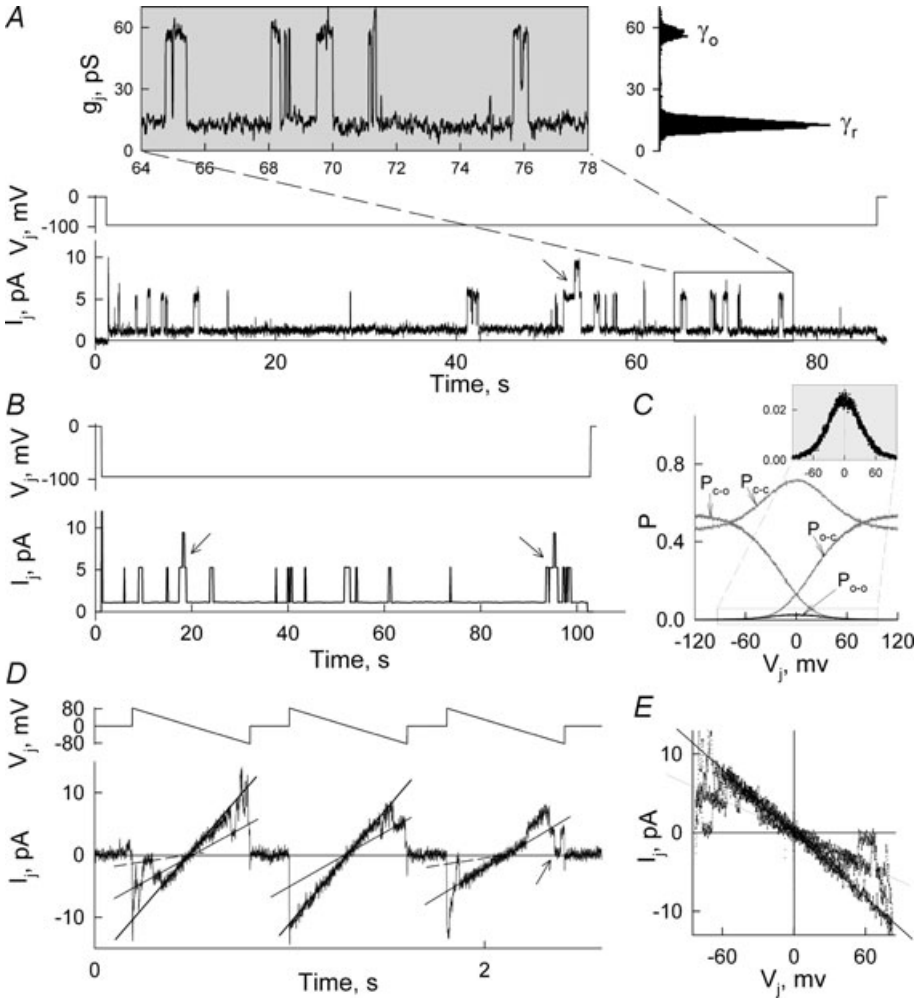

Figure 3. Unitary gating events in HeLaCx57-EGFP cell pairs
A, an example of I_j record during V_j step of −95 mV in a cell pair with low coupling at control conditions (∼0.1 nS). Most gating transitions are between open (γ_o) and residual states (γ_{res}). The inset shows calculated g_j for the time window between 64 and 78 s. Frequency histogram (top-right) reveals two major peaks of 11 ± 0.85 and 57 ± 1.35 pS, which correspond to γ_{res} and γ_o, respectively. *B–C*, simulation of V_j-gating in the junction containing 200 homotypic GJ channels using the model of contingent gating. I_j trace in *B* was obtained in response to V_j step of −95 mV (upper trace). *C*, probability of channels to dwell in different states (O–O, C–O, O–C and C–C) depending on V_j. The black line shows $P_{o\text{-}o}$ (see the inset), while grey lines show $P_{c\text{-}o}$, $P_{o\text{-}c}$, and $P_{c\text{-}c}$. *D*, I_j recording from cell pair exhibiting unitary gating events in response to three consecutive V_j ramps of ±80 mV. *E*, I_j–V_j plot of data showed in *D*. Continuous lines are drawn over I_j traces corresponding to one and two open channels, and dashed lines correspond to the residual state.

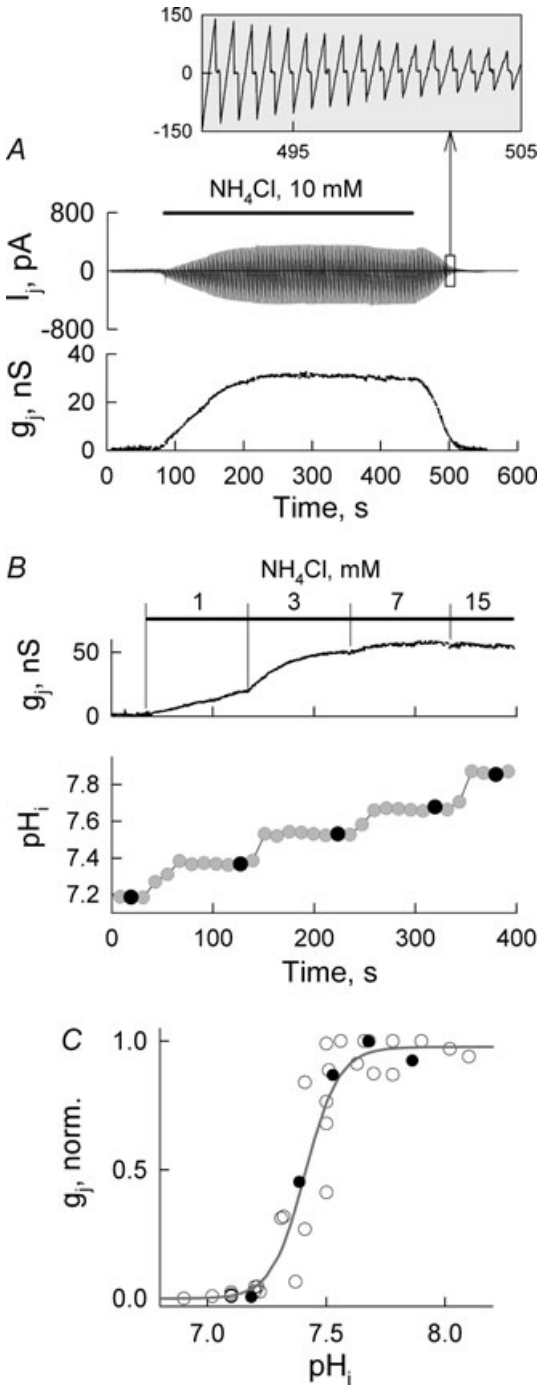

Figure 4. pH_i-dependent modulation of junctional conductance
A, dynamics of I_j and g_j measured by applying repeated V_j ramps of ±20 mV (enlarged I_j responses to V_j ramps are shown in the inset) in response to applications of NH_4Cl (10 mM). *B*, g_j and pH_i measurements in one cell pair after application of 1, 3, 7 and 15 mM of NH_4Cl. *C*, summarized g_j–pH_i relationship in which the continuous line is a fitting curve to the Hill equation; $pK_a = 7.41 \pm 0.02$ and the Hill coefficient of 5.9 ± 0.5 ($n = 6$). Filled circles are from the experiment shown in *B*.

(see the inset). To change pH_i without changing pH_o, we used ammonium chloride (NH_4Cl) added to the modified Krebs–Ringer (MKR) solution (Swietach & Vaughan-Jones, 2005). Application of NH_4Cl (10 mM), which typically raised pH_i for ∼0.6 units, increased g_j from 0.8 to ∼30 nS in ∼100 s. In 31 examined cell pairs application of NH_4Cl (10 mM) increased g_j on average from 0.41 ± 0.15 to 43.6 ± 6.7 nS.

To find out how g_j depends on pH_i, we loaded cells with BCECF (for more details see http://probes.invitrogen.com), a fluorescent indicator for pH_i, and applied different concentrations of NH_4Cl. We measured g_j values at different concentrations of NH_4Cl (Fig. 4*B*). Figure 4*C* summarizes the g_j–pH_i relationship. Data fitting with Hill's equation revealed that $pK_a = 7.41 \pm 0.02$ and the Hill coefficient, $n = 5.9 \pm 0.5$ ($n = 6$), where pK_a is the pH at half maximum of g_j, and n characterizes cooperativity of the H^+ ions and their binding sites on the GJ channel.

To determine whether intracellular alkalization affects V_j-gating, we examined changes of g_j–V_j dependence in nine experiments. To reduce the time needed to measure g_j–V_j dependences after application of increasing concentrations of NH_4Cl, we examined V_j-gating by applying slow voltage ramps of one polarity, as shown in Fig. 5*A*. We found that in parallel with g_j increase, the V_j-gating sensitivity was substantially reduced. Figure 5*B* shows that application of 1 and subsequently 6 mM of NH_4Cl increased g_j from ∼0.9 to 4 and 27 nS, respectively. Grey numbers (1–7) attached to g_j–V_j plots shown in Fig. 5*B*–*D* correspond to the numbers attached to V_j ramps shown in Fig. 5*A*. Continuous grey lines in Fig. 5*B* show fitting curves of g_j–V_j plots by using the model of contingent gating (Paulauskas *et al.* 2009). During the fitting process, we assumed that each experimental g_j–V_j plot has a symmetric counterpart at positive V_j values and that for both hemichannels $\gamma_{h,o} = 114$ pS. Figure 5*C* shows dependencies of $P_{o\text{-}o}$ on V_j for g_j–V_j plots shown in *B*. Under control conditions $P_{o\text{-}o}$ at $V_j = 0$ mV was very low (∼0.02) and increased with application of NH_4Cl, approaching 1 for g_j–V_j plot no. 3 and remaining at this level for all other g_j–V_j plots. In addition, $P_{o\text{-}o}$–V_j plots became less V_j sensitive. The fitting of the data with the model allowed us to define $V_{h,o}$ and the number of functional GJ channels for each g_j–V_j plot. Figure 5*D* shows that over time $V_{h,o}$ increased from −16 to 98 mV (filled circles) and N_f increased from 220 to 490 GJ channels (open circles). Therefore, an increase of g_j during alkalization is caused by changes of both $P_{o\text{-}o}$ and N_f. The same tendency under intracellular alkalization was found in all nine other experiments including the one shown in the online supplementary figure, Fig. S1.

It is always a concern that the increase in g_j can lead to some reduction of V_j-gating sensitivity due to a series resistance effect (Wilders & Jongsma, 1992). In regards

to this, we would like to emphasize that even at equal $g_{j,max}$ values in no. 6 and no. 7 (Fig. 5*B*) g_j–V_j plots (~27 nS) they show a substantial difference in sensitivity to V_j-gating. Similar differences in V_j-gating sensitivity can be seen in the supplemental Fig. S1 between g_j–V_j plot no. 8 and plots nos 9–11 exhibiting the same $g_{j,max}$. Although it is not possible to exclude fully an effect of series resistance on V_j-gating, our data allow us to conclude that intracellular alkalization indeed reduces sensitivity of V_j-gating.

Gating of Cx57-EGFP/Cx45 heterotypic gap junction channels

Gating polarity, which defines whether AHCs close at negative or positive potential on their cytoplasmic side, is one of the fundamental properties of GJs that cannot be determined in homotypic GJs. This can be done in cell pairs where Cx57 forms heterotypic channels with another Cx isoform with the already established gating polarity; e.g. Cx45 exhibits a negative gating polarity (Bukauskas *et al.* 2002*b*). We examined gating properties of heterotypic junctions in a coculture of HeLaCx57-EGFP and HeLaCx45 cells pre-labelled with DAPI. This allowed us to select heterologous cell pairs for the experiments. Figure 6*A* shows that under control conditions (pH_i 7.2) as well as during application of NH_4Cl, I_j response evoked by voltage ramps applied to the cell expressing Cx45 was asymmetric. We observed this I_j/V_j asymmetry in all five experiments and found that application of NH_4Cl (2 mM) increased g_j 2.0 ± 0.3-fold ($n = 5$). Figure 6*B* (black dots) shows the averaged g_j–V_j dependence that was obtained

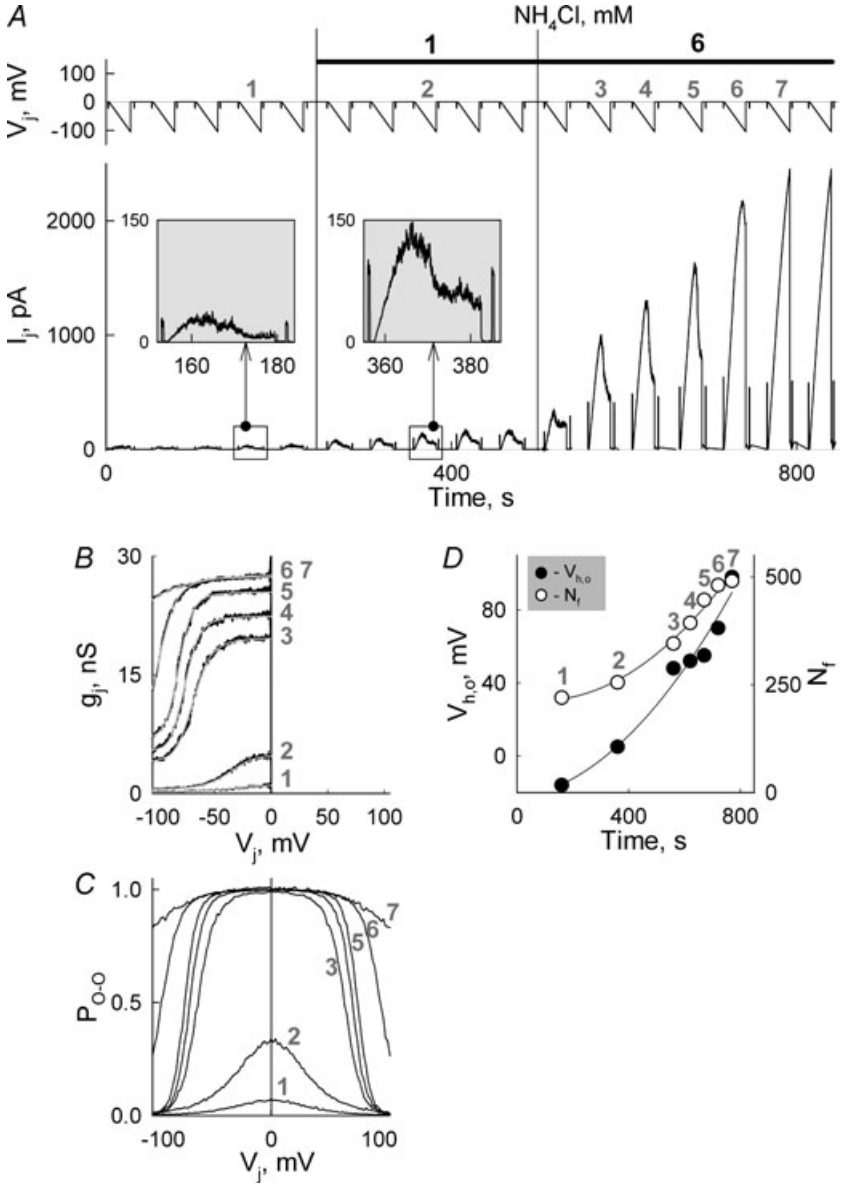

Figure 5. Dynamics of V_j-gating during intracellular alkalization in HeLaCx57-EGFP cell pairs
A, I_j recording in response to repeated V_j ramps from 0 to −110 mV before and during application of NH_4Cl (1 and 6 mM). Voltage steps of −20 mV were used to measure g_j in between voltage ramps. The insets show I_j responses on an enlarged scale to voltage ramps before and after application of 1 mM NH_4Cl. *B*, g_j–V_j dependencies calculated from V_j and I_j records shown in *A*. Grey lines show fitting curves obtained by using the model of contingent gating for each experimental g_j–V_j plot. Grey numbers in *B*–*D* attached to different plots correspond to numbers of V_j ramps shown in *A*. *C*, $P_{o\text{-}o}$ dependence on V_j for different g_j–V_j plots. *D*, changes of $V_{h,o}$ (open circles) and N_f (filled circles) over time during recordings shown in (*A*). Continuous lines show regression curves of the second order (continuous lines).

by overlapping normalized g_j–V_j plots ($n = 8$) measured under control conditions. The white line is a fitting curve obtained from the model of contingent gating assuming that $\gamma_{h,Cx57} = 114$ pS (see above), $\gamma_{h,Cx45} = 57$ pS (Valiunas, 2002) and gating polarity of Cx57 is negative, i.e. the same as for Cx45. Assuming that the gating polarity of Cx57 is positive, then the simulated g_j–V_j plot (see black line obtained using the same parameters as for the white line) deviates substantially from the experimental data. Thus, we demonstrate that Cx57 channels exhibit a negative gating polarity.

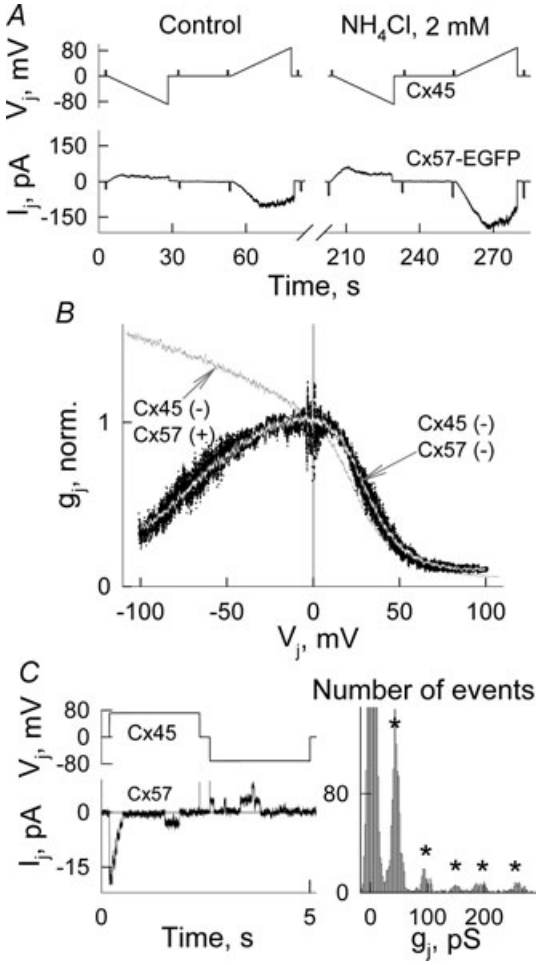

Figure 6. Voltage gating of Cx57-EGFP/Cx45 heterotypic gap junction channels
A, I_j response in cells expressing Cx57-EGFP evoked by V_j ramps applied to the cell expressing Cx45 shows I_j/V_j asymmetry. Application of NH_4Cl (2 mM) increased g_j ∼2-fold. *B*, an averaged g_j–V_j dependence (black dots) that was obtained by overlapping normalized g_j–V_j plots measured under control conditions. The white line inside experimental points is a fitting curve obtained from the model of contingent gating assuming that the gating polarity of Cx57 is negative, i.e. the same as for Cx45. The black line shows the simulated g_j–V_j plot with the same parameters of the model for white line but assuming that the gating polarity of Cx57 is positive. *C*, I_j recordings in cell expressing Cx57-EGFP that exhibit unitary gating events in response to positive and negative V_j steps applied to the cell expressing Cx45, and the histogram of g_j data obtained from the I_j/V_j ratio, suggesting that unitary conductance of Cx45–Cx57 heterotypic junction is ∼49 pS.

Figure 6*C* shows I_j recordings in a heterologous cell pair expressing Cx57-EGFP that exhibit unitary gating events in response to positive and negative V_j steps applied to the cell expressing Cx45. The histogram of g_j data shows that the distance between the peaks is ∼49 pS. Therefore, unitary conductance of the Cx45–Cx57 heterotypic junction is, as expected, in between the single channel conductances of Cx45 and Cx57 homotypic junctions, i.e. 32 (Bukauskas *et al.* 2002*b*) and 57 pS, respectively.

The major goal of these studies was to establish the gating polarity of Cx57. In doing so, we found that Cx45–Cx57 heterotypic GJs under control conditions exhibit junctional coupling of ∼2 nS i.e., substantially higher than in Cx57 homotypic junctions. In addition, alkalization increased g_j of Cx45–Cx57 heterotypic junctions assuming that this was caused mainly by Cx57 hemichannel. However, we did not pursue this direction more in depth because we do not know either the exact g_j–pH dependence of Cx45 or whether heterotypic GJs configuration modulates sensitivity to pH or V_j-gating.

Permeability studies

To assess the permeability of GJ channels, we measured dye transfer and g_j in HeLaCx57-EGFP cell pairs exhibiting at least one JP. In these studies, the pipette filled with dye is typically attached to cell-1 and the pipette without dye attached to cell-2. The patch in cell-1 was opened to fill it with dye and observe dye transfer to cell-2. Approximately 10 min later, the patch in cell-2 was open to measure g_j in dual whole-cell voltage clamp mode. This allowed us to avoid problems related to dye flux into the pipette of cell-2 during dye transfer measurements.

We demonstrate that Cx57-EGFP GJ channels are permeable to LY, AF^{350}, EtBr and DAPI, but not PrI (Fig. 7*A*). At least five cell pairs were examined for each dye. In the experiments where no dye transfer occurred during the first 5 min of recording, cells were exposed to 5 mM of NH_4Cl, which typically increases g_j. We found difficulties detecting LY and PrI transfer under normal perfusion conditions, and only after application of NH_4Cl for ∼30 min could we conclude that LY but not PrI permeates Cx57-EGFP GJ channels.

To quantify dye permeability, we only used dyes that remain largely unbound in the cytoplasm and do not change their quantum efficiency after binding. Most of the positively charged dyes bind to nucleotides and change their quantum efficiency substantially. To assess the junctional permeability (P_j) of negatively charged AF^{350}, we measured changes in fluorescence intensities in both cells, FI_1 and FI_2, over time. As indicated above and in Fig. 7*A*, AF^{350} permeates Cx57-EGFP GJ channels,

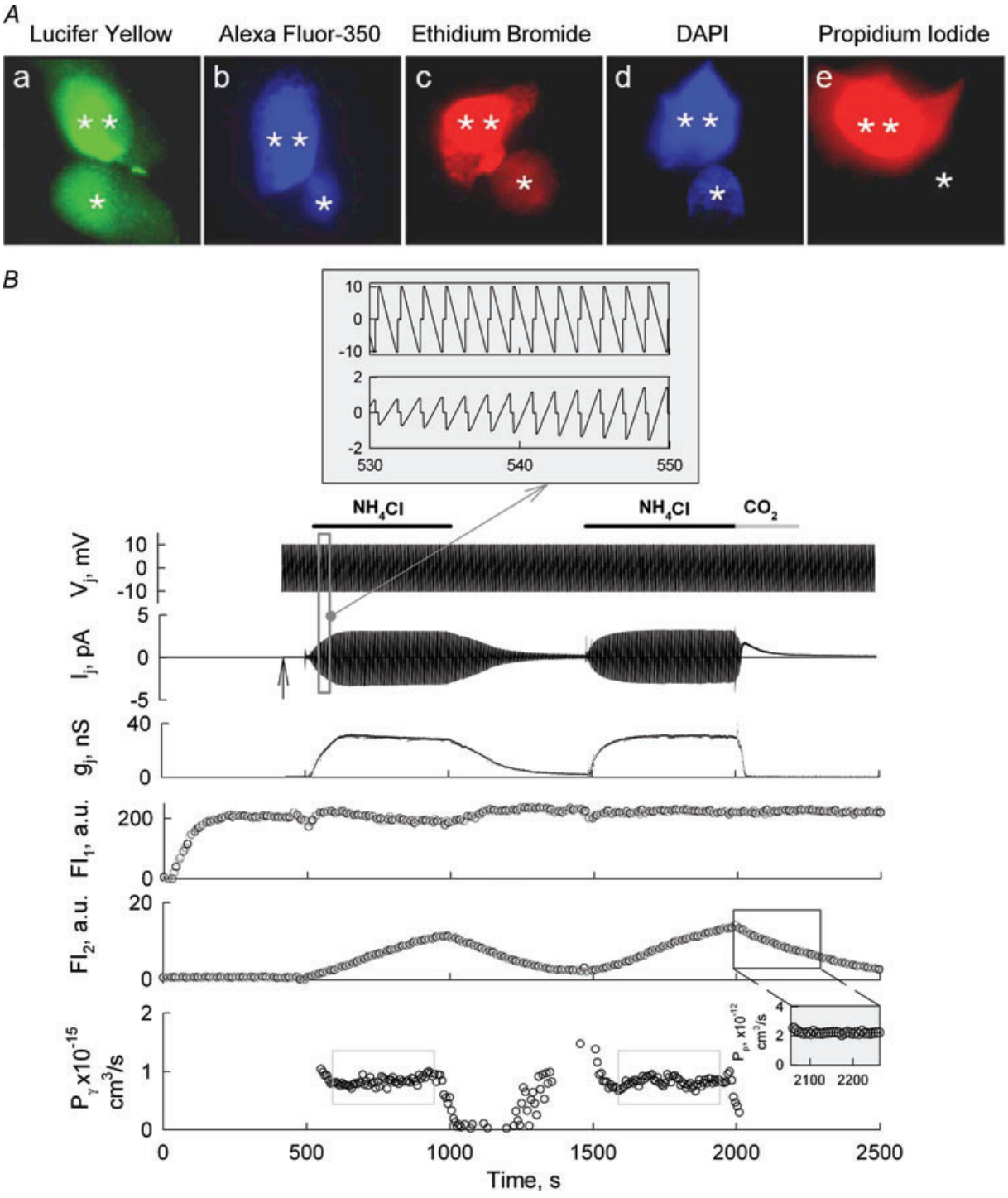

Figure 7. Permeability of Cx57-EGFP gap junction channels to dyes
A, representative images illustrating LY (*a*), AF^{350} (*b*), EtBr (*c*) and DAPI (*d*) but not PrI (*e*) permeate GJ channels. Images were recorded ∼10 min after opening the patch in cell-1 with pipette filled with dye (indicated by two asterisks). Dye acceptor cell is shown by one asterisk. *B*, Cx57-EGFP single channel permeability to AF^{350}. Two consecutive applications of NH_4Cl (10 mM) were used to increase g_j. The grey bar shows CO_2 application used to measure P_p that characterizes AF^{350} permeability from cell-2 (dye recipient cell) to patch pipette-2. Repeated V_j ramps of ±12 mV were used to measure I_j (see the inset). The patch to cell-1 was open at the beginning of the recording. The vertical arrow shows the moment when the patch was open in cell-2 to measure I_j. FI_1 and FI_2 traces show dynamics of fluorescence intensities in cell-1 and cell-2, respectively. P_γ trace shows the single channel permeability.

but it was problematic to quantify this permeability due to the low g_j. To overcome this problem, we increased g_j by applying NH_4Cl. Figure 7*B* shows one of six experiments in which we measured P_j and single channel permeability (P_γ) by combining electrophysiological and imaging techniques. Soon after opening the patch in cell-1, fluorescence intensity started to increase in cell-1 but there were no detectable changes in cell-2. At ∼120 s, the patch was opened in cell-2 (see vertical arrow) allowing the measurement of junctional conductance by applying repeated ramps of ±12 mV; an example of I_j response to V_j ramps is shown in the top inset. Initially g_j was around 0.1 nS suggesting a very low P_o at $V_j = 0$ mV. To increase g_j, cells were exposed two times to NH_4Cl (10 mM; see horizontal bars). Each application resulted in an increase of I_j followed by FI_2 increase. The second application of NH_4Cl was followed by exposure to 100% CO_2 (see grey horizontal bar) that resulted in full uncoupling.

We used the time window of 2050–2260 s (see the inset on FI_2 trace), when junctional conductance was blocked by CO_2, to estimate the parameter P_p, characterizing dye permeability from cell-2 to pipette-2. For more details see Methods and eqn (7). We found that in this experiment $P_p = 2.2 \times 10^{-11}$ cm^3 s^{-1}. P_p depends presumably on the size of the open patch at the very tip of the patch pipette and among the six experiments it varied between 1.2 and 2.9×10^{-11} cm^3 s^{-1}. The bottom trace in Fig. 7*B* shows calculated P_γ by using eqn (8). To find P_γ, we used the data inside grey rectangles, i.e. during periods with noticeable g_j values. We found that on average $P_\gamma = 0.95 \pm 0.09 \times 10^{-15}$ cm^3 s^{-1} ($n = 6$). All P_γ measurements were performed at repeated ramps of small amplitude and with the absence of a permanent V_j, and therefore transjunctional electrical field did not affect P_γ. As it was reported earlier, AF^{350}, LY and cAMP do not permeate the residual state of Cx43 and Cx46 (Bukauskas *et al.* 2002*a*; Qu & Dahl, 2002). Thus, we assume that AF^{350} does not permeate the residual state of Cx57 GJ channels that exhibit even lower conductance than Cx43 or Cx46 and measured P_γ should indeed reflect permeability of the open state.

In summary, P_γ of Cx57-EGFP GJ channels is 24-fold higher than that of Cx30.2 and 6-, 35- and 90-fold lower than those of Cx45, Cx40, and Cx43 GJ channels, respectively (see Rackauskas *et al.* (2007) for P_γ values of Cx30.2, Cx45, Cx40 and Cx43 GJs). The ratios between γ_o values of Cx57 and Cx30.2, Cx45, Cx40 and Cx43 GJ channels are ∼6, 1.7, 0.4 and 0.5, respectively. Thus, permeability of GJs to metabolites is not directly proportional to their unitary conductances.

Functional efficiency of Cx57 gap junction channels

Our data show that measured g_j was much lower than expected assuming that all GJ channels assembled into junctional plaques would be functional. To address this question quantitatively, we performed a series of experiments similar to those previously used to determine the functional efficiency of Cx43 GJs (Bukauskas *et al.* 2000). Initially, we searched for cell pairs showing JPs in contact regions where cells overlap and the JP can be seen *en face*, as illustrated in Fig. 1*C*. Imaging at different focal planes showed that some of the selected JPs were large, oriented parallel to the focal plane. To obtain fluorescence per unit area, light emission was integrated over a given area of uniform fluorescence and background fluorescence was measured outside the JP. We used JPs of several micrometres in diameter to ensure that fluorescence in the centre of the plaque, where the region of interest (ROI) is located, was homogeneous. We evaluated fluorescence per unit area in *en face* JPs (F_{JP}) in arbitrary fluorescent units, a.u. (background subtracted). In all experiments, we used the same objective, light intensity and exposure time for fluorescence imaging. We estimated the fluorescence produced by a single GJ channel (F_γ) using F_{JP} and the packing density of GJ channels previously described by other groups. We assumed that each Cx57-EGFP GJ channel occupied 100 nm^2 (corresponding to 10 nm centre-to-centre in a square array) as an approximation of values seen in electron microscope studies of junctions in fixed tissues (Caspar *et al.* 1977; Peracchia, 1977) or of isolated JP imaged in aqueous media by atomic force microscopy (Lal *et al.* 1995). On average F_{JP} was equal to 1980 ± 52 a.u. per 1 μm^2 ($n = 12$). From the ratio 1980 a.u./10000 GJ channels per 1 μm^2, we found that $F_\gamma = 0.2$ a.u. In addition, we found that HeLaCx43-EGFP also exhibited very similar F_γ when measured under the same conditions (Bukauskas *et al.* 2000).

In combined imaging and electrophysiological studies, we measured g_j and the total fluorescence intensity of JPs (F_T) independent of their spatial orientation. F_T was estimated by measuring the total fluorescence in the ROI enclosing JP as shown in Fig. 1*B* (background subtracted). The total number of physical GJ channels (N_T) present in each JP was determined from the ratio $N_T = F_T/F_\gamma$. When $P_o = 1$, the number of fully open GJ channels at any given time (functional channels $= N_f$) for each cell pair can be determined as the ratio of total junctional conductance at $V_j = 0$ mV to a single GJ channel conductance, $N_f = g_j/\gamma$. The fraction of operating GJ channels (K) can be determined as the ratio between functional channels and total number of channels at any given time, $K = N_f/N_T = g_j F_\gamma / F_T \gamma$.

We found that application of NH_4Cl (10 mM) that typically raised pH from 7.2 to ∼7.8 increased g_j on average from 0.41 ± 0.15 to 43.6 ± 6.7 nS ($n = 13$). Our earlier studies showed that EGFP fluorescence increased when pH increased from 5.5 to ∼7 and was close to constant at a pH in the range of 7 to 9 (see supplements of Bukauskas *et al.* (2006)). Therefore, at pH_i in the range

of 7.2 to 7.8, dependence of EGFP fluorescence on pH_i should not affect evaluations of F_T and F_γ.

Our data show that $P_o = \sim 1$ under exposure of cells to 10 mM of NH_4Cl (see Fig. 5*C* and Fig. S1*D* in the Supplemental Material). Thus, we can assume that all functional GJ channels are fully open with $\gamma = 57$ pS. Consequently, we found that under these conditions $N_f = 43.6/0.057 = 765$ channels and $K = 0.023 \pm 0.006$ ($n = 13$), which is ~6.5-fold lower than K reported for Cx43-EGFP (Bukauskas *et al.* 2000). An assessment of K at pH = 7.2 is more complicated because as we showed earlier $P_{o\text{-}o}$ is very low and measured g_j is a sum of conductances of channels residing in the fully open state and the substate or residual state. Therefore, it would be too speculative to define K at pH 7.2. If some g_j increase during application of 10 mM of NH_4Cl is due to ~2-fold increase in the number of functional GJ channels (see Fig. 5*D* and Fig. S1*F*), then K at control conditions should be equal to $0.023/2 = \sim 0.012$. Thus, we speculate that under control conditions ~1% of Cx57-EGFP GJ channels are functional.

Cx57 unapposed hemichannels

To study whether Cx57-EGFP forms functional UHCs, we examined the uptake of fluorescent dyes using time-lapse imaging (see Methods). A co-culture of HeLa parental and HeLaCx57-EGFP cells were plated in a 35 mm thin glass-bottomed Petri dish. The dish was placed inside the CO_2 microincubator on the top of 40× or 60× oil objectives. During imaging, cells were exposed to 5 μM of DAPI and 0.5 μM of EtBr or 2 μM of PrI. Emission wavelengths of DAPI and EtBr or PrI do not overlap. We did not find any statistically significant differences in EtBr and DAPI uptakes between HeLa parental and HeLaCx57-EGFP cells under exposure to either DMEM (see Fig. 8*A–C*) or to MKR solution containing 2 mM Ca^{2+}. An exposure of cells to a normal MKR solution containing 5 mM of NH_4Cl did not affect the rate of dye uptake. Such concentration of NH_4Cl typically increases pH_i by ~0.4 units.

HeLaCx57-EGFP cells exposed to a Ca-free MKR solution showed ~5-fold increase in the rate of DAPI uptake, while the rate of EtBr and PrI uptake remained unaffected. Ca^{2+}-free conditions not only increased DAPI uptake but also induced cell swelling, which became evident after ~1 h. NH_4Cl (5 mM) added to the Ca-free solution accelerated DAPI uptake and shortened the lag time to ~30 min for cell swelling. HeLa parental cells did not show cell swelling or an increase in the rate of DAPI uptake. Figure 8*D–E* shows that cells expressing Cx57-EGFP (green) but not HeLa parental cells become round in shape, swell and demonstrate enhanced uptake of DAPI (blue) when exposed to Ca^{2+}-free MKR solution containing 5 mM NH_4Cl for 25 min. Swelling of cells that lasted for ~10–20 min typically led to a rapid

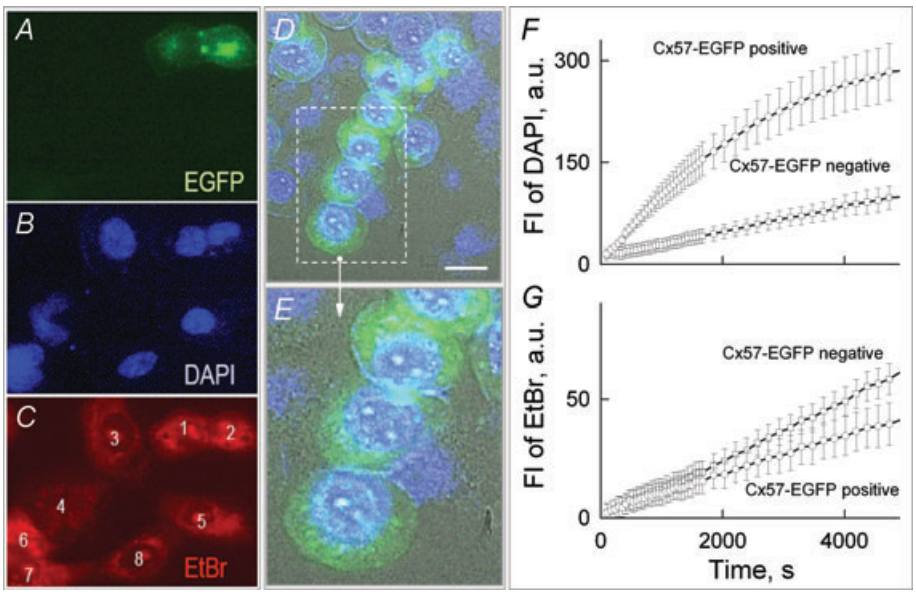

Figure 8. Dye uptake in co-cultured HeLaCx57-EGFP and HeLa parental cells
A–C, fluorescence images of cells recorded 60 min after exposure to DAPI (5 μM) and EtBr (0.5 μM) added to DMEM. There was no noticeable difference in uptake of DAPI (*B*) and EtBr (*C*) between two cells expressing (shown in green) and not expressing Cx57-EGFP. *D–E*, cells expressing Cx57-EGFP (green) but not HeLa parental cells demonstrate enhanced uptake of DAPI (blue) and become round in shape ~25 min after exposure to a Ca^{2+}-free (no added Ca^{2+}) MKR solution containing 5 mM of NH_4Cl. *F–G*, dynamics of DAPI (*F*) and EtBr (*G*) uptake at $[Ca^{2+}]_o = 100$ μM in MKR solution; FI was measured in arbitrary units (a.u.) by subtracting background intensity.

increase in the uptake of EtBr and PrI, presumably due to damage of the plasma membrane integrity. Figure 8*F–G* shows the dynamics of DAPI (*F*) and EtBr (*G*) uptake at $[Ca^{2+}]_o = 0.1$ mM in MKR solution. Figure 8*F* shows that the rate of DAPI uptake is ∼3-fold higher in cells expressing Cx57-EGFP than in cells not exhibiting EGFP signal. There was no statistically significant difference in EtBr uptake among expressing and non-expressing EGFP cells (Fig. 8*G*). At $[Ca^{2+}]_o = 0.3$ mM, the rate of DAPI uptake increased approximately 1.5-fold and at $[Ca^{2+}]_o = 0.5$ mM there was almost no effect on the rate of DAPI uptake (not shown). Therefore, our data show that Cx57-EGFP UHCs are mainly closed under normal conditions and open under lessening $[Ca^{2+}]_o$ to 0.3 mM or below. Interestingly, UHCs are permeable to DAPI (279 Da; $z = +2$) but not to dyes with higher molecular mass, EtBr (314 Da; $z = +1$) and PrI (415 Da; $z = +2$), suggesting that the size but not the net charge is a limiting factor for permeation of UHC.

Does tagged EGFP makes a difference?

To study whether tagged EGFP affects properties of Cx57 GJ channels and UHCs, experiments were performed in HeLa cells transfected with the pMJ-Cx57IRES-eGFP vector resulting in co-expression of wild-type Cx57 (Cx57WT) and untagged EGFP that distributes virtually homogeneously inside the cells. All six examined cell pairs showed a g_j increase after application of NH_4Cl and its recovery to initial values during the washout period. Figure 9*A* shows that in one of these cell pairs shortly after application of NH_4Cl (5 mM) g_j increased from ∼0.2 nS and reached a steady state at ∼8 nS. The g_j was measured by applying repeated ±20 mV ramps to one cell of the cell pair. The inset shows I_j responses to voltage ramps during an initial period of NH_4Cl application. I_j responses to positive and negative ∼70 mV voltage steps show moderate (∼25%) decay. Studies of g_j–V_j dependence by using long voltage ramps also revealed a decrease in V_j gating sensitivity under exposure to NH_4Cl. Figure 9*B*

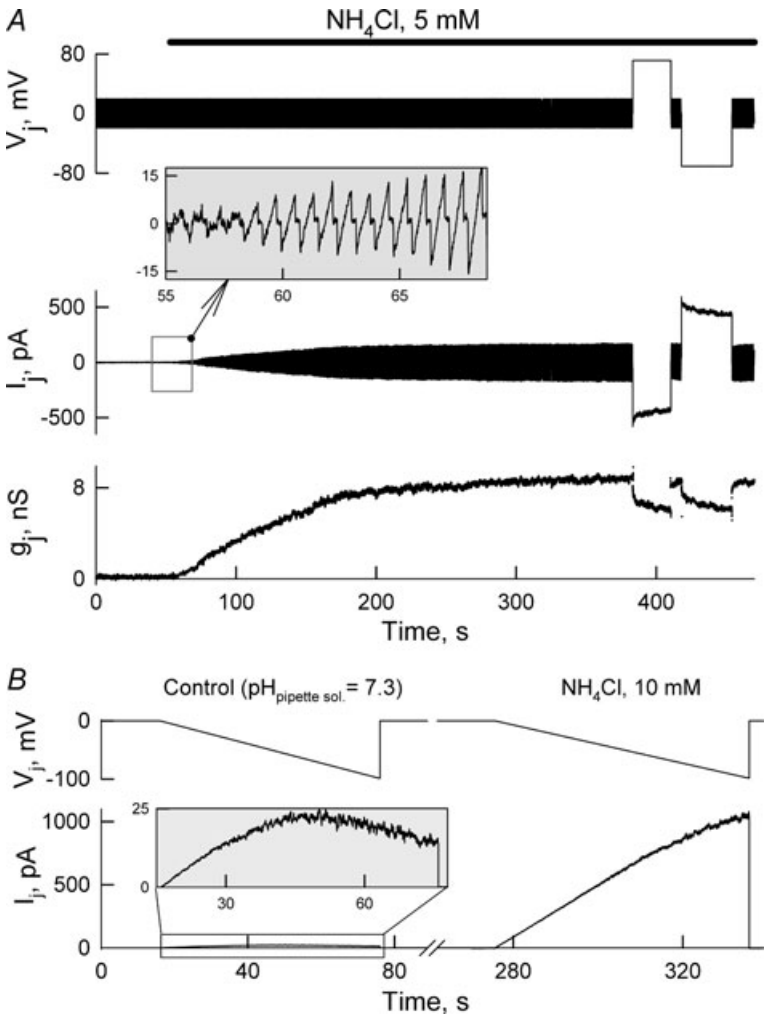

Figure 9. pH-dependent modulation of g_j in HeLa cells expressing wild-type Cx57 and untagged EGFP
A, intracellular alkalization with NH_4Cl (5 mM) increased g_j from ∼0.2 nS to ∼8 nS. MKR solution containing 2 mM of $CaCl_2$ was used in this experiment. g_j was measured by applying repeated V_j ramps of ±20 mV. The inset shows I_j responses to V_j ramps during an initial period of NH_4Cl application. I_j responses to positive and negative ∼70 mV voltage steps show moderate (∼25%) decay. *B*, I_j trace measured in response to 60 s long V_j ramps from 0 to −100 mV shows well expressed V_j-gating under control conditions at $pH_{pipette-sol} = 7.3$, while under exposure to NH_4Cl, the I_j–V_j relationship is almost linear indicating almost no V_j-gating.

demonstrates that in response to 60 s long V_j ramps from 0 to −100 mV, the I_j trace shows well expressed V_j-gating under control conditions at $pH_{pipette-sol.} = 7.3$ compared to a nearly linear change under exposure to NH_4Cl. We observed no difference between a single GJ channel conductance of Cx57-EGFP and Cx57WT co-expressed with an untagged EGFP (not shown). In addition, imaging of cocultures of HeLa parental and HeLaCx57 cells revealed no difference in EtBr and DAPI uptake under normal conditions and a significant increase in dye uptake only by cells expressing Cx57WT under exposure to Ca^{2+}-free medium (not shown). In summary, we conclude that Cx57WT and Cx57-EGFP exhibit similar V_j-gating, g_j–pH_i relationship and function of UHCs depending on $[Ca^{2+}]_o$.

Discussion

Different hypotheses have been proposed to explain how GJ channels and UHCs in horizontal cells are involved in the processing of light-modulated signals in the retina. Despite extensive studies performed on this matter, the role of Cx57, the major Cx expressed in mouse horizontal cells, remains disputable.

Biophysical properties and pH-dependent modulation of Cx57 gap junction channels

Combined fluorescence imaging and dual whole-cell patch clamp methods allowed us to conclude that HeLa cells expressing Cx57 exhibited relatively weak electrical cell–cell coupling under control conditions and that only a small fraction of GJ channels assembled into JPs function at any given time (∼1%). Several factors can determine this small ratio: (1) some GJ channels assembled into JPs may not be functional, e.g. GJ channels that are in the process of internalization are closed permanently, (2) newly assembled GJ channels need some time to mature, (3) open channel probability is very low, (4) interaction with other proteins that may modulate function of GJs, etc.

It is commonly accepted that the cytoplasm is slightly acidified (∼0.2 pH units) compared to extracellular milieu. We found that at pH_i 7.2 Cx57 GJ channels exhibit very low P_o. By how much does pH_i in horizontal cells differ from 7.2? There are only a few reports showing that pH_i in isolated horizontal cells under normal conditions is between 7.3 and 7.4 (Haugh-Scheidt & Ripps, 1998; Takahashi *et al.* 1993; Dixon *et al.* 1996). In addition, pH_i can vary substantially among different tissues and cell types, and numerous factors can affect pH_i. For example, synchronous neuronal spiking at high frequency can cause changes in intracellular and extracellular pH within seconds (Chesler, 2003). Changes in pH_o (which may exert an effect on pH_i) have also been suggested to play a role in the modulation of coupling between horizontal cells in retinas of rabbits, fish and mice (DeVries & Schwartz, 1989; Hampson *et al.* 1992; Jouhou *et al.* 2007*b*). Depolarization of fish horizontal cells reduced pH_o in their immediate surrounding by activating the release of H^+ via the voltage-sensitive H^+-pump (V-ATPase) supporting the hypothesis that the feedback from horizontal cells to photoreceptors could be proton mediated (Jouhou *et al.* 2007*b*). Moreover, a significant reduction of dye transfer in horizontal cells of the rabbit retina has been described when pH_o was reduced to 7.2 (Hampson *et al.* 1994). Our data show that the pK_a of Cx57 GJs is 7.41 ± 0.02, which is close to the pH_i measured experimentally in horizontal cells, and the Hill coefficient is 5.9 ± 0.1, which is close to a number of Cxs in the hemichannels. This suggests that the g_j between horizontal cells can be efficiently regulated by small changes in pH_i around 7.4 where the steepness of the g_j–pH_i relationship is maximal (Fig. 4*C*). We found that ∼100-fold increase of g_j when pH_i increased from ∼7.2 to 7.8 was caused by an increase of $P_{o\text{-}o}$ and N_f (see Fig. 5*C*–*D* and supplemental Fig. S1*D*–*E*).

We demonstrate that Cx45–Cx57 heterotypic junctions exhibit an increase of coupling in response to alkalization as well. We assume that for this heterotypic junction Cx57 AHC is a limiting factor determining this g_j increase because it demonstrates higher sensitivity to pH_i than Cx45 exhibiting $pK_a = \sim 7$ (Stergiopoulos *et al.* 1999). If P_o of Cx57 AHC is equal to 0.1 (see $P_{o\text{-}c}$ or $P_{c\text{-}o}$ traces in Fig. 3*C*) and we assume that P_o of Cx45 AHC is equal to 1 (for reasons of simplicity), then P_o of Cx45–Cx57 GJs should be ∼0.1 (0.1×1), while P_o of Cx57 homotypic junction should be ∼0.01 (0.1×0.1). This may explains why Cx45–Cx57 heterotypic junctions exhibit higher g_j than Cx57 homotypic junctions under control conditions.

At this point it would be difficult to envision the mechanism of pH action on g_j. For Cx43 it was predicted that its C-terminus is involved in the pH-dependent closing of GJ channels and the pK_a for both Cx40 and Cx43 is equal to 6.7 (Morley *et al.* 1997; Gu *et al.* 2000). Interestingly, compared to Cx43, Cx57 has 12 more histidine residues in the C-terminus, which may explain the enhanced sensitivity to pH_i. However, the Hill coefficient for Cx43 ($n = 5.5$) (Stergiopoulos *et al.* 1999) does not differ evidently from Cx57 ($n = 5.9$) and the molecular events that determine pK_a and the Hill coefficient for Cx57 are yet to be resolved. Protonation of histidine residues in the second half of the cytoplasmic loop and its interaction with the C-terminus may also cause pH-sensitive gating (Delmar *et al.* 2004). There is one histidine residue in the second half of the Cx57 cytoplasmic loop surrounded by several lysine residues (not typical for Cx43) that may also be involved in pH-sensitive gating. However, further studies must be

carried out to relate pH sensitivity of Cx57 with its structure.

Earlier studies of Cx57 with the incorrect sequence (longer C-terminus) (Manthey *et al.* 1999) also showed surprisingly low cell–cell coupling with g_j in the range of 0.2–2.5 nS. At that time the g_j–pH_i dependence was not examined, but equally low g_j as well as similarity in V_j-gating allows us to assume that Cx57 with a longer C-terminus has a similar g_j–pH_i relationship to Cx57 with the corrected C-terminus.

Our single GJ channel conductance measurements of the open state (57 pS) are in concert with γ_o values of 50–60 pS found in horizontal cells of teleost (McMahon *et al.* 1989) and bass retinas (Lu & McMahon, 1996). Single GJ channel conductance of Cx45–Cx57 heterotypic junction is, as expected, in between γ_o values of Cx45 and Cx57 homotypic junctions, i.e. 32 (Bukauskas *et al.* 2002*b*) and 57 pS, respectively. We observed no difference between γ_o values of Cx57-EGFP and Cx57WT co-expressed with an untagged EGFP (not shown). However, measured γ_o is higher than that reported earlier (Manthey *et al.* 1999) for Cx57 with the longer C-terminus, ∼28 pS. At this point, we expect that the difference in the sequence of the C-terminus between old (incorrect) and new (corrected) versions of Cx57 explains the difference in the unitary conductance. In addition, tagged-EGFP did not affect gating properties of Cx57 GJ channels. This conclusion is based on the presence of fast and slow phases during g_j recovery from V_j-gating and the residual conductance measured macroscopically (see Fig. 2*E*) and at the single channel level (Fig. 3*A*–*D*). Data obtained by examining Cx57–Cx45 heterotypic junctions (Fig. 6) allowed us to conclude that Cx57 GJ channels have a negative gating polarity, i.e. the same as Cx30.2 (Kreuzberg *et al.* 2005), Cx36 (F. F. Bukauskas, unpublished observations) and Cx45 (Bukauskas *et al.* 2002*b*) that are also expressed in the retina. This suggests that Cx57 UHC also exhibit a negative gating polarity and their open probability tends to increase by increasing positivity on the cytoplasmic side.

Our permeability studies show that Cx57 GJ channels are permeable to LY, AF^{350}, EtBr and DAPI, but not to PrI. Thus, Cx57 GJ channels are largely non-selective for the net charge of the permeable molecule; rather, the size of the dye determines its permeability. For example, both DAPI and PrI have two positive charges, but PrI is greater in molecular mass (415 *vs.* 279 Da for ionic forms) and does not permeate Cx57 GJs. Our data show, that the single Cx57-EGFP GJ channel exhibits 24-fold higher permeability for AF^{350} than mCx30.2 and 6-, 35- and 90-fold lower than Cx45, Cx40, and Cx43 GJ channels, respectively (Rackauskas *et al.* 2007). Interestingly, despite the fact that single channel conductance of Cx57 GJs is ∼2-fold higher than that of Cx45, P_γ for AF^{350} is ∼6-fold lower. The lack of correlation between single channel conductance and permeability may imply that in Cx57, GJ channel constriction site(s) are narrower resulting in lower permeability to molecules comparable in size with numerous metabolites.

Potential implications for the Ca^{2+}-dependent modulation of Cx57 unapposed hemichannels

We demonstrate that Cx57 UHCs can open after reducing $[Ca^{2+}]_o$ at moderate levels, ∼0.3 mM. This reduction of $[Ca^{2+}]_o$ can be physiologically relevant in the narrow interstitial space of the ribbon synaptic complex where photoreceptors interact with bipolar and horizontal cells. Moreover, our data show that the opening of Cx57 UHCs by low $[Ca^{2+}]_o$ could be potentiated by intracellular alkalization. Recently, no Cx57 immunoreactivity was found in dendritic tip membranes of horizontal cells. It was concluded that Cx57 UHCs are absent in the triad synapse of photoreceptors, bipolar cells and horizontal cells (Janssen-Bienhold *et al.* 2009). Typically, UHCs residing in the plasma membrane tend to distribute diffusely; otherwise they should be anchored to scaffolding proteins or their diffusion should be limited by barriers similar to those present in endothelial cells. If neither of these factors was demonstrated, it would be difficult to exclude the possibility that their concentration is below the limit of resolution for immunoreactivity studies.

In the dark, photoreceptors are depolarized, release glutamate continuously, and keep the horizontal cells depolarized. It is well known that depolarization can increase the open probability of UHCs (Contreras *et al.* 2003). In addition, the reduction of $[Ca^{2+}]_o$ in the synaptic cleft, induced by Ca^{2+} entry in the photoreceptors during dark (Rabl & Thoreson, 2002), may further enhance the open probability of UHCs. Therefore, Cx57 UHCs may open during dark and increase an exchange of ions and metabolites between the cytoplasm and the extracellular milieu. Light stimulation hyperpolarizes photoreceptors, reduces glutamate release and hyperpolarizes horizontal cells. Presumably, hyperpolarization of horizontal cells should tend to close UHCs due to their negative gating polarity shown in this study (see above).

It has been proposed that horizontal cells generate a negative feedback signal to photoreceptors upon light stimulation (Kaneko & Tachibana, 1986; Kamermans *et al.* 2001; Hirasawa & Kaneko, 2003; Vessey *et al.* 2005; Cadetti & Thoreson, 2006; Jouhou *et al.* 2007*a*; Davenport *et al.* 2008). This negative feedback could be abolished experimentally by gap junction blockers (Kamermans *et al.* 2001; Verweij *et al.* 2003; Pottek *et al.* 2003). However, the loss of Cx57 expression in Cx57 knockout mice had no influence on this negative feedback (Shelley *et al.* 2006), and caused changes in neither spatial tuning nor light adaptation of retinal ganglion cells (Dedek *et al.* 2008).

Data demonstrating possible compensatory changes in the Cx57 knockout mice are lacking. Hence, involvement of Cx57 UHCs in the feedback from horizontal cells to photoreceptors in the wild-type mouse retina remains disputable.

We show that Ca^{2+}-free conditions not only increased the rate of DAPI uptake but also induced cell swelling, which was followed by necrotic transformations. The latency for cell swelling and necrosis decreased from 1 h to 30 min after adding NH_4Cl to the Ca^{2+}-free MKR solution. We found that it was more difficult to culture and maintain stable cell lines expressing Cx57-EGFP or Cx57WT than cell lines expressing other Cx isomers, such as Cx26, Cx32, Cx36, Cx40, Cx43, etc. During the trypsinization procedure, when the cells are exposed to very low $[Ca^{2+}]_o$, a high fraction of cells expressing Cx57-EGFP or Cx57 swell and become necrotic. Only a relatively small fraction of cells, typically those forming numerous JPs, survived the trypsinization procedure. We assume that in cells forming more JPs, a lesser fraction of UHCs are in the plasma membrane, and therefore fewer UHCs can be open during the trypsinization procedure. We found that adding 0.5 mM Ca^{2+} to the trypsin solution improved cell survival. Thus, our data show that Cx57 UHCs are mainly closed under normal conditions and open at moderately low $[Ca^{2+}]_o$. A future reduction of $[Ca^{2+}]_o$ up to several micromolar leads to an extensive opening of Cx57 UHCs resulting in cell death. In addition, among HeLa cell lines stably expressing different Cxs isoforms fused with GFPs, only HeLaCx57-EGFP cells show necrotic transformations under Ca^{2+}-free conditions or during trypsinization. Therefore, we suggest that the increase in dye uptake under reduction of $[Ca^{2+}]_o$ can be mainly attributed to the opening of Cx57 UHCs.

Our data support the notion that Cx57 forms functional UHCs in horizontal cells of mouse retina similarly to Cxs expressed in horizontal cells of catfish, skate and zebrafish retinas (DeVries & Schwartz, 1992; Malchow *et al.* 1993; Shields *et al.* 2007; Zoidl *et al.* 2004). Strong pH_i-gating of Cx57 GJs in a physiologically relevant range provides evidence to support experimental data showing pH regulation of centre–surround antagonism and the modulation of the receptive field size. Finally, our data show that there is no need to reach an extremely low concentration of $[Ca^{2+}]_o$ to open Cx57 UHCs.

References

Baldridge WH, Ball AK & Miller RG (1987). Dopaminergic regulation of horizontal cell gap junction particle density in goldfish retina. *J Comp Neurol* **265**, 428–436.

Becker D, Bonness VV & Mobbs P (1998). Cell coupling in the retina: patterns and purpose. *Cell Biol Intern* **22**, 781–792.

Bennett MV, Barrio LC, Bargiello TA, Spray DC, Hertzberg E & Saez JC (1991). Gap junctions: new tools, new answers, new questions. *Neuron* **6**, 305–320.

Bukauskas FF, Bukauskiene A, Bennett MV & Verselis VK (2001). Gating properties of gap junction channels assembled from connexin43 and connexin43 fused with green fluorescent protein. *Biophys J* **81**, 137–152.

Bukauskas FF, Bukauskiene A & Verselis VK (2002*a*). Conductance and permeability of the residual state of connexin43 gap junction channels. *J Gen Physiol* **119**, 171–186.

Bukauskas FF, Bukauskiene A, Verselis VK & Bennett MVL (2002*b*). Coupling asymmetry of heterotypic connexin 45/connexin 43-EGFP gap junctions: Properties of fast and slow gating mechanisms. *Proc Natl Acad Sci U S A* **99**, 7113–7118.

Bukauskas FF, Jordan K, Bukauskiene A, Bennett MV, Lampe PD, Laird DW & Verselis VK (2000). Clustering of connexin 43-enhanced green fluorescent protein gap junction channels and functional coupling in living cells. *Proc Natl Acad Sci U S A* **97**, 2556–2561.

Bukauskas FF, Kreuzberg M, Rackauskas M, Bukauskiene A, Bennett MVL, Verselis VK & Willecke K (2006). Properties of mouse connexin 30.2 and human connexin 31.9 hemichannels: implications for atrioventricular conduction in the heart. *Proc Natl Acad Sci U S A* **103**, 9726–9731.

Bukauskas FF & Verselis VK (2004). Gap junction channel gating. *Biochim Biophys Acta* **1662**, 42–60.

Cadetti L & Thoreson WB (2006). Feedback effects of horizontal cell membrane potential on cone calcium currents studied with simultaneous recordings. *J Neurophysiol* **95**, 1992–1995.

Caspar DL, Goodenough DA, Makowski L & Phillips WC (1977). Gap junction structures. I. Correlated electron microscopy and x-ray diffraction. *J Cell Biol* **74**, 605–628.

Chesler M (2003). Regulation and modulation of pH in the brain. *Physiol Rev* **83**, 1183–1221.

Ciolofan C, Lynn BD, Wellershaus K, Willecke K & Nagy JI (2007). Spatial relationships of connexin36, connexin57 and zonula occludens-1 in the outer plexiform layer of mouse retina. *J Neurosci* **148**, 473–488.

Contreras JE, Saez JC, Bukauskas FF & Bennett MV (2003). Gating and regulation of connexin 43 (Cx43) hemichannels. *Proc Natl Acad Sci U S A* **100**, 11388–11393.

Davenport CM, Detwiler PB & Dacey DM (2008). Effects of pH buffering on horizontal and ganglion cell light responses in primate retina: evidence for the proton hypothesis of surround formation. *J Neurosci* **28**, 456–464.

Deans MR & Paul DL (2001). Mouse horizontal cells do not express connexin26 or connexin36. *Cell Commun Adhes* **8**, 361–366.

Dedek K, Pandarinath C, Alam NM, Wellershaus K, Schubert T, Willecke K, Prusky GT, Weiler R & Nirenberg S (2008). Ganglion cell adaptability: does the coupling of horizontal cells play a role? *PLoS ONE* **3**, e1714.

Delmar M, Coombs W, Sorgen P, Duffy HS & Taffet SM (2004). Structural bases for the chemical regulation of Connexin43 channels. *Cardiovasc Res* **62**, 268–275.

DeVries SH & Schwartz EA (1989). Modulation of an electrical synapse between solitary pairs of catfish horizontal cells by dopamine and second messengers. *J Physiol* **414**, 351–375.

DeVries SH & Schwartz EA (1992). Hemi-gap-junction channels in solitary horizontal cells of the catfish retina. *J Physiol* **445**, 201–230.

Dixon DB, Takahashi K, Bieda M & Copenhagen DR (1996). Quinine, intracellular pH and modulation of hemi-gap junctions in catfish horizontal cells. *Vision Res* **36**, 3925–3931.

Dobrowolski R, Sommershof A & Willecke K (2007). Some oculodentodigital dysplasia-associated Cx43 mutations cause increased hemichannel activity in addition to deficient gap junction channels. *J Membr Biol* **219**, 9–17.

Ek-Vitorin JF & Burt JM (2005). Quantification of gap junction selectivity. *Am J Physiol Cell Physiol* **289**, C1535–1546.

Gallemore RP, Li JD, Govardovskii VI & Steinberg RH (1994). Calcium gradients and light-evoked calcium changes outside rods in the intact cat retina. *Vis Neurosci* **11**, 753–761.

Gu H, Ek-Vitorin JF, Taffet SM & Delmar M (2000). Coexpression of connexins 40 and 43 enhances the pH sensitivity of gap junctions: a model for synergistic interactions among connexins. *Circ Res* **86**, E98–E103.

Hampson EC, Vaney DI & Weiler R (1992). Dopaminergic modulation of gap junction permeability between amacrine cells in mammalian retina. *J Neurosci* **12**, 4911–4922.

Hampson EC, Weiler R & Vaney DI (1994). pH-gated dopaminergic modulation of horizontal cell gap junctions in mammalian retina. *Proc Biol Sci* **255**, 67–72.

Harris AL (2001). Emerging issues of connexin channels: biophysics fills the gap. *Q Rev Biophys* **34**, 325–427.

Haugh-Scheidt L & Ripps H (1998). pH regulation in horizontal cells of the skate retina. *Exp Eye Res* **66**, 449–463.

Hille B (2001). *Ionic Channels of Excitable Membranes*. Sinauer Associates, Sunderland, MA.

Hirasawa H & Kaneko A (2003). pH changes in the invaginating synaptic cleft mediate feedback from horizontal cells to cone photoreceptors by modulating Ca^{2+} channels. *J Gen Physiol* **122**, 657–671.

Hombach S, Janssen-Bienhold U, Söhl G, Schubert T, Büssow H, Ott T, Weiler R & Willecke K (2004). Functional expression of connexin57 in horizontal cells of the mouse retina. *Eur J Neurosci* **19**, 2633–2640.

Janssen-Bienhold U, Schultz K, Gellhaus A, Schmidt P, Ammermuller J & Weiler R (2001). Identification and localization of connexin26 within the photoreceptor-horizontal cell synaptic complex. *Vis Neurosci* **18**, 169–178.

Janssen-Bienhold U, Trümpler J, Hilgen G, Schultz K, De Sevilla Müller LP, Sonntag S, Dedek K, Dirks P, Willecke K & Weiler R (2009). Connexin57 is expressed in dendro-dendritic and axo-axonal gap junctions of mouse horizontal cells and its distribution is modulated by light. *J Comp Neurol* **513**, 363–374.

Jouhou H, Yamamoto K, Homma A, Hara M, Kaneko A & Yamada M (2007*a*). Depolarization of isolated horizontal cells of fish acidifies their immediate surrounding by activating V-ATPase. *J Physiol* **585**, 401–412.

Jouhou H, Yamamoto K, Iwasaki M & Yamada M (2007*b*). Acidification decouples gap junctions but enlarges the receptive field size of horizontal cells in carp retina. *Neurosci Res* **57**, 203–209.

Kamermans M & Fahrenfort I (2004). Ephaptic interactions within a chemical synapse: hemichannel-mediated ephaptic inhibition in the retina. *Curr Opin Neurobiol* **14**, 531–541.

Kamermans M, Fahrenfort I, Schultz K, Janssen-Bienhold U, Sjoerdsma T & Weiler R (2001). Hemichannel-mediated inhibition in the outer retina. *Science* **292**, 1178–1180.

Kamermans M & Spekreijse H (1999). The feedback pathway from horizontal cells to cones. A mini review with a look ahead. *Vision Res* **39**, 2449–2468.

Kaneko A & Tachibana M (1986). Effects of gamma-aminobutyric acid on isolated cone photoreceptors of the turtle retina. *J Physiol* **373**, 443–461.

Kreuzberg MM, Deuchars J, Weiss E, Schober A, Sonntag S, Wellershaus K, Draguhn A & Willecke K (2008). Expression of connexin30.2 in interneurons of the central nervous system in the mouse. *Mol Cell Neurosci* **37**, 119–134.

Kreuzberg MM, Sohl G, Kim J, Verselis VK, Willecke K & Bukauskas FF (2005). Functional properties of mouse connexin30.2 expressed in the conduction system of the heart. *Circ Res* **96**, 1169–1177.

Kuffler SW (1953). Discharge patterns and functional organization of mammalian retina. *J Neurophysiol* **16**, 37–68.

Lal R, John SA, Laird DW & Arnsdorf MF (1995). Heart gap junction preparations reveal hemiplaques by atomic force microscopy. *Am J Physiol Cell Physiol* **268**, C968–C977.

Lu C & McMahon DG (1996). Gap junction channel gating at bass retinal electrical synapses. *Vis Neurosci* **13**, 1049–1057.

Malchow RP, Qian H & Ripps H (1993). Evidence for hemi-gap junctional channels in isolated horizontal cells of the skate retina. *J Neurosci Res* **35**, 237–245.

Manthey D, Bukauskas F, Lee CG, Kozak CA & Willecke K (1999). Molecular cloning and functional expression of the mouse gap junction gene connexin-57 in human HeLa cells. *J Biol Chem* **274**, 14716–14723.

Maxeiner S, Dedek K, Janssen-Bienhold U, Ammermuller J, Brune H, Kirsch T, Pieper M, Degen J, Kruger O, Willecke K & Weiler R (2005). Deletion of connexin45 in mouse retinal neurons disrupts the rod/cone signalling pathway between AII amacrine and ON cone bipolar cells and leads to impaired visual transmission. *J Neurosci* **25**, 566–576.

McMahon DG (1994). Modulation of electrical synaptic transmission in zebrafish retinal horizontal cells. *J Neurosci* **14**, 1722–1734.

McMahon DG, Knapp AG & Dowling JE (1989). Horizontal cell gap junctions: single-channel conductance and modulation by dopamine. *Proc Natl Acad Sci U S A* **86**, 7639–7643.

Mills SL & Massey SC (1995). Differential properties of two gap junctional pathways made by aII amacrine cells. *Nature* **377**, 734–737.

Morley GE, Ek-Vitorin JF, Taffet SM & Delmar M (1997). Structure of connexin43 and its regulation by pH_i. *J Cardiovasc Electrophysiol* **8**, 939–951.

Paulauskas N, Pranevicius M, Pranevicius H & Bukauskas FF (2009). A four-state model of contingent gating of gap junction channels containing two 'fast' gates sensitive to transjunctional voltage. *Biophys J* (in press).

Peracchia C (1977). Gap junctions. Structural changes after uncoupling procedures. *J Cell Biol* **72**, 628–641.

Pottek M, Hoppenstedt W, Janssen-Bienhold U, Schultz K, Perlman I & Weiler R (2003). Contribution of connexin26 to electrical feedback inhibition in the turtle retina. *J Comp Neurol* **466**, 468–477.

Qu Y & Dahl G (2002). Function of the voltage gate of gap junction channels: selective exclusion of molecules. *Proc Natl Acad Sci U S A* **99**, 697–702.

Rabl K & Thoreson WB (2002). Calcium-dependent inactivation and depletion of synaptic cleft calcium ions combine to regulate rod calcium currents under physiological conditions. *Eur J Neurosci* **16**, 2070–2077.

Rackauskas M, Verselis VK & Bukauskas FF (2007). Permeability of homotypic and heterotypic gap junction channels formed of cardiac connexins mCx30.2, Cx40, Cx43, and Cx45. *Am J Physiol Heart Circ Physiol* **293**, H1729–1736.

Saez JC, Berthoud VM, Branes MC, Martinez AD & Beyer EC (2003). Plasma membrane channels formed by connexins: their regulation and functions. *Physiol Rev* **83**, 1359–1400.

Shelley J, Dedek K, Schubert T, Feigenspan A, Schultz K, Hombach S, Willecke K & Weiler R (2006). Horizontal cell receptive fields are reduced in connexin57-deficient mice. *Eur J Neurosci* **23**, 3176–3186.

Shields CR, Klooster J, Claassen Y, Ul-Hussain M, Zoidl G, Dermietzel R & Kamermans M (2007). Retinal horizontal cell-specific promoter activity and protein expression of zebrafish connexin 52.6 and connexin 55.5. *J Comp Neurol* **501**, 765–779.

Sohl G, Maxeiner S & Willecke K (2005). Expression and functions of neuronal gap junctions. *Nat Rev Neurosci* **6**, 191–200.

Stergiopoulos K, Alvarado JL, Mastroianni M, Ek-Vitorin JF, Taffet SM & Delmar M (1999). Hetero-domain interactions as a mechanism for the regulation of connexin channels. *Circ Res* **84**, 1144–1155.

Swietach P & Vaughan-Jones RD (2005). Relationship between intracellular pH and proton mobility in rat and guinea-pig ventricular myocytes. *J Physiol* **566**, 793–806.

Takahashi K, Dixon DB & Copenhagen DR (1993). Modulation of a sustained calcium current by intracellular pH in horizontal cells of fish retina. *J Gen Physiol* **101**, 695–714.

Teranishi T, Negishi K & Kato S (1983). Dopamine modulates S-potential amplitude and dye-coupling between external horizontal cells in carp retina. *Nature* **301**, 243–246.

Teranishi T, Negishi K & Kato S (1984). Dye coupling between amacrine cells in carp retina. *Neurosci Lett* **51**, 73–78.

Trexler EB, Bukauskas FF, Bennett MVL, Bargiello TA & Verselis VK (1999). Rapid and direct effects of pH on connexins revealed by the connexin46 hemichannel preparation. *J Gen Physiol* **113**, 721–742.

Valiunas V (2002). Biophysical properties of connexin-45 gap junction hemichannels studied in vertebrate cells. *J Gen Physiol* **119**, 147–164.

Valiunas V, Beyer EC & Brink PR (2002). Cardiac gap junction channels show quantitative differences in selectivity. *Circ Res* **91**, 104–111.

Vaney DI & Weiler R (2000). Gap junctions in the eye: evidence for heteromeric, heterotypic and mixed-homotypic interactions. *Brain Res Brain Res Rev* **32**, 115–120.

Verselis V, White RL, Spray DC & Bennett MV (1986). Gap junctional conductance and permeability are linearly related. *Science* **234**, 461–464.

Verweij J, Hornstein EP & Schnapf JL (2003). Surround antagonism in macaque cone photoreceptors. *J Neurosci* **23**, 10249–10257.

Vessey JP, Stratis AK, Daniels BA, Da Silva N, Jonz MG, Lalonde MR, Baldridge WH & Barnes S (2005). Proton-mediated feedback inhibition of presynaptic calcium channels at the cone photoreceptor synapse. *J Neurosci* **25**, 4108–4117.

Weiler R, Pottek M, He S & Vaney DI (2000). Modulation of coupling between retinal horizontal cells by retinoic acid and endogenous dopamine. *Brain Res Brain Res Rev* **32**, 121–129.

Wilders R & Jongsma HJ (1992). Limitations of the dual voltage clamp method in assaying conductance and kinetics of gap junction channels. *Biophys J* **63**, 942–953.

Zoidl G, Bruzzone R, Weickert S, Kremer M, Zoidl C, Mitropoulou G, Srinivas M, Spray DC & Dermietzel R (2004). Molecular cloning and functional expression of zfCx52.6: a novel connexin with hemichannel-forming properties expressed in horizontal cells of the zebrafish retina. *J Biol Chem* **279**, 2913–2921.

Author contribution

N.P.-P., S.S., V.A.S., K.W. and F.F.B. designed the experiments; N.P.-P. and F.F.B. performed most of the experiments; S.S. made all constructs; N.P.-P. and F.F.B. planned and performed the analysis of the data; N.P.-P., S.S., V.A.S., K.W. and F.F.B. wrote, revised and approved the final version of the paper. All experiments were carried out at the Department of Neuroscience, Albert Einstein College of Medicine.

Acknowledgements

We thank Angele Bukauskiene for excellent technical assistance and Eileen Zenz for proofreading the manuscript. This work was supported by National Institutes of Health Grants R01 NS036706 and R01 HL084464 to F.F.B. and by a grant of the German research Association (Wi270/31-1) to K.W.